IVYSPRING INTERNATIONAL PUBLISHER

Theranostics

2026; 16(12): 6576-6599. doi: 10.7150/thno.130266

Review

The CXCR4-targeted theranostics era: a comprehensive review of a decade of progress (2015–2025)

Biao Yang[1,2,3], Wenzhu Hu[1,2,3], Xiao Zhang[1,2,3], Yongkang Gai[1,2,3], Rui An[1,2,3], Chunxia Qin[1,2,3], Mengting Li[1,2,3]✉, Xiaoli Lan[1,2,3]✉

1. Department of Nuclear Medicine, Union Hospital, Tongji Medical College, Huazhong University of Science and Technology, Wuhan 430022, China.
2. Hubei Province Key Laboratory of Molecular Imaging, Wuhan 430022, China.
3. Key Laboratory of Biological Targeted Therapy, the Ministry of Education, Wuhan 430022, China.

✉ Corresponding authors: Xiaoli Lan, MD, Ph.D., Address: No. 1277 Jiefang Ave, Wuhan 430022, Hubei Province, China, Telephone/Fax number: 86-27-83692633, E-mail: xiaoli_lan@hust.edu.cn; lxl730724@hotmail.com. Mengting Li, MD, Ph.D., Address: No. 1277 Jiefang Ave, Wuhan 430022, Hubei Province, China, Telephone/Fax number: 86-27-83692633, E-mail: limengtingtjmu@163.com.

Received: 2025.12.19; Accepted: 2026.03.19; Published: 2026.05.01

Abstract

Over the past decade, theranostics targeting the chemokine receptor CXCR4 have evolved from a promising concept into a clinical reality, revolutionizing the management of a diverse spectrum of diseases. This paradigm shift has been fueled by the development of [^{68}Ga]Pentixafor, a high-affinity PET radiotracer that enables the precise, non-invasive visualization of CXCR4 expression *in vivo*. Its diagnostic prowess extends beyond conventional oncology, demonstrating superior performance to [^{18}F]FDG in hematologic malignancies and offering critical decision-making insights for endocrine disorders and inflammatory conditions. Seamlessly completing the theranostic loop, the therapeutic counterparts [^{177}Lu]/[^{90}Y]Pentixather deliver targeted radiotherapy to CXCR4-expressing tissues, with pioneering applications in advanced multiple myeloma and acute myeloid leukemia establishing a compelling safety and efficacy profile. While challenges in target heterogeneity and toxicity persist, the future of CXCR4-targeted theranostics is bright, poised for advancement through combinatorial immunotherapies, alpha-emitting radionuclides, and artificial intelligence-driven patient stratification. This review comprehensively synthesizes a decade of progress, affirming CXCR4-targeted theranostics as a cornerstone of precision medicine that faithfully adheres to the "see what you treat, treat what you see" philosophy.

Keywords: CXCR4, theranostics, Pentixafor, positron emission tomography, targeted radionuclide therapy

1. Introduction

Chemokine receptor CXCR4, a class A G protein-coupled receptor, mediates diverse physiological and pathological processes through its interaction with the endogenous ligand CXCL12 [1,2]. This signaling axis plays crucial roles in cancer progression, immune surveillance, and stem cell homing [3]. Under physiological conditions, CXCR4 is constitutively expressed on T lymphocytes and macrophages, where it regulates lymphocyte trafficking and facilitates the migration, homing, and retention of hematopoietic stem cells within the bone marrow niche [4]. Moreover, CXCR4 serves as a coreceptor for human immunodeficiency virus type 1 (HIV-1), collaborating with CD4 to enable viral entry into host T cells [5–7].

In oncological contexts, CXCR4 is frequently overexpressed in a wide spectrum of malignancies, including hematologic neoplasms such as multiple myeloma (MM) and acute myeloid leukemia (AML), as well as solid tumors like breast, prostate, and pancreatic cancers [8–12]. Such dysregulated expression is closely associated with enhanced metastatic potential, therapeutic resistance, and unfavorable prognosis. Mechanistically, CXCR4-CXCL12 signaling promotes tumor cell survival, proliferation, and dissemination [13]. Within the tumor microenvironment, CXCR4 is also expressed on various immune cells, including

dendritic cells, regulatory T cells, and $CD8^+$ T cells, where it participates in shaping immunosuppressive landscapes [14]. Beyond oncology, this axis is implicated in the pathogenesis of inflammatory disorders, cardiovascular diseases, and infectious conditions, though the full scope of its molecular mechanisms remains to be fully elucidated [15–17]. Compared to other G protein-coupled receptors, CXCR4 presents itself as a particularly compelling target for molecular theranostics. This is due to its frequent and marked overexpression in a wide range of diseases, its efficient ligand-induced internalization and its well-established role in driving key disease pathways such as metastasis, cell survival, and therapy resistance (Figure 1).

Owing to its central role in disease mechanisms, CXCR4 has garnered significant interest as a target for molecular imaging and targeted radionuclide therapy. A key milestone was achieved in 2015 with the development of [^{68}Ga]Pentixafor at the Technical University of Munich [19]. This radiotracer is based on a high-affinity cyclic pentapeptide scaffold (cyclo(D-Tyr^1-[NMe]-D-Orn^2-Arg^3-2-Nal^4-Gly^5)) and enables non-invasive assessment of CXCR4 expression via positron emission tomography (PET). In an initial proof-of-concept human study involving four patients with lymphoproliferative diseases, [^{68}Ga]Pentixafor PET demonstrated high imaging contrast and clinical feasibility, paving the way for broader translational applications. Subsequent efforts have focused on developing therapeutic counterparts such as ^{177}Lu- and ^{90}Y-labeled Pentixather, which are designed to deliver cytotoxic radiation to CXCR4-expressing tumors [20].

Notably, the field of CXCR4-targeted theranostics has expanded to include a broader range of ligand development. For example, the literature has reported novel CXCR4 antagonists with higher affinity, whose innovative design strategies and promising preclinical profiles pave the way for next-generation radiopharmaceuticals [21,22]. Meanwhile, clinical research is no longer limited to Pentixafor. Recent studies have summarized early clinical results of alternative CXCR4-targeted tracers based on different scaffolds [23,24]. Collectively, these advances demonstrate that CXCR4 imaging has evolved into a versatile platform with multiple tracer options, each potentially possessing unique pharmacokinetic or binding properties. In this review, we summarize key preclinical advances in the development of CXCR4-directed radiopharmaceuticals and highlight emerging clinical applications of [^{68}Ga]Pentixafor for diagnostic imaging and [^{177}Lu]/[^{90}Y]Pentixather for endoradiotherapy in malignant and selected benign diseases.

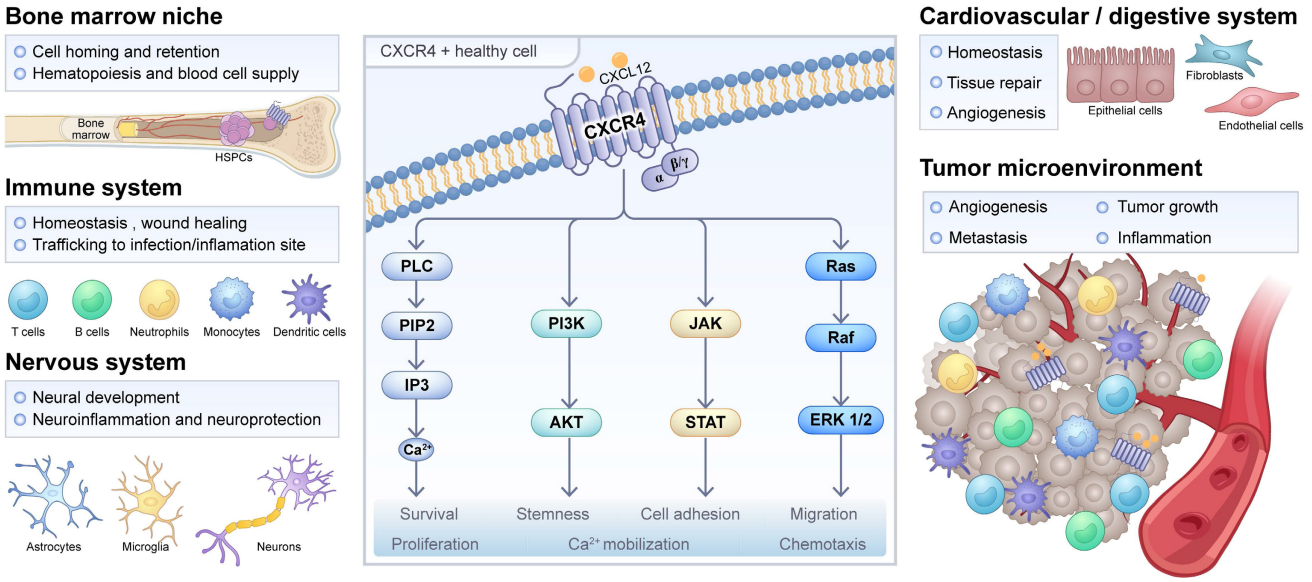

Figure 1. CXCR4 signaling in physiological or pathological processes. The physiological role of CXCR4 is listed for hematopoietic stem and progenitor cells (HSPCs) in the bone marrow and other cell types in the immune, nervous, cardiovascular, and digestive systems. Meanwhile, the pathological role of CXCR4 in inflammation, infection, injury repair, and the tumor microenvironment is also indicated. The CXCR4/CXCL12 interaction and the activated main signaling pathways, namely PLC, PI3K/Akt, JAK/STAT, and MAPK, are shown in the middle, along with their downstream cellular responses. Adapted with permission from [18], copyright © 2025, Springer Nature.

2. Preclinical studies of CXCR4-targeted radiopharmaceuticals

Given the critical role of CXCR4 in mediating cancer metastasis, it was identified as a promising therapeutic target as early as 2011 [25]. A novel high-affinity cyclic CXCR4 ligand, [^{68}Ga]Pentixafor (cyclo(D-Tyr^{1}-[NMe]-D-Orn^{2}-[4-(aminomethyl)benzoic acid,^{68}Ga-DOTA]-Arg^{3}-2-Nal^{4}-Gly^{5})), was developed and systematically validated both *in vitro* and *in vivo* using nude mouse models bearing metastatic OH1 human small cell lung cancer (SCLC) xenografts. This radiotracer demonstrated exceptional *in vivo* stability, highly specific tumor uptake, and minimal off-target accumulation in non-tumor tissues, thereby establishing a solid foundation for the development of CXCR4-targeted radiopharmaceuticals. Subsequent research has evaluated derivatives labeled with alternative radiometals (e.g., AMD- and T140-based analogs) across various tumor models [19,26–28]. A growing body of evidence supports [^{68}Ga]Pentixafor PET imaging as a highly translational approach for assessing CXCR4 expression *in vivo*, both in preclinical models and clinical cancer populations [29–32]. This diagnostic advancement has facilitated the parallel development of corresponding therapeutic agents—notably [^{177}Lu]/[^{90}Y]Pentixather—enabling integrated theranostic strategies for personalized CXCR4-directed therapy.

The efficacy of [^{68}Ga]Pentixafor as a leading CXCR4-targeted imaging probe has been rigorously validated through comprehensive preclinical evaluations across multiple cancer models. Wester *et al.* employed two lymphoma models, Daudi (a human Burkitt's lymphoma cell line with high CXCR4 expression) and SU-DHL-8 (a human large B-cell lymphoma cell line with low CXCR4 expression), to demonstrate that [^{68}Ga]Pentixafor exhibits high affinity and selectivity for human CXCR4, along with favorable pharmacokinetic properties [19]. In MM research, NOD SCID mice xenografted with MM.1S and OPM-2 cells underwent sequential [^{18}F]FDG and [^{68}Ga]Pentixafor PET imaging [32]. Notably, [^{68}Ga]Pentixafor achieved significantly higher mean tumor-to-background ratios (TBRs) in both xenograft models compared to [^{18}F]FDG, highlighting its superior diagnostic performance. Additionally, [^{68}Ga]Pentixafor PET imaging enabled precise visualization of heterogeneous CXCR4 expression levels in tumor xenografts derived from patient-derived xenograft models of T-cell acute lymphoblastic leukemia and AML [33]. Researchers have further employed *in vitro* cell-binding assays and the chorioallantoic membrane xenograft model to evaluate the diagnostic potential of [^{68}Ga]Pentixafor in colorectal cancer imaging, expanding its preclinical applications across both hematologic malignancies and solid tumors [34].

Beyond its established applications in cancer models, the noninvasive diagnostic potential of [^{68}Ga]Pentixafor has been extensively investigated in inflammatory diseases, including atherosclerosis, heart failure, and acute myocardial infarction (AMI). A preclinical study in experimental rabbit models demonstrated the tracer's capability to detect CXCR4 expression on inflammatory cells within atherosclerotic plaques [30]. Compared to normal control arteries, significantly elevated radiotracer uptake was observed in atherosclerotic lesions of the abdominal aorta (mean TBR = 1.95 ± 0.51 *vs*. 1.22 ± 0.25; $p < 0.05$) and right carotid artery (mean TBR = 1.24 ± 0.38 *vs*. 0.96 ± 0.37; $p < 0.05$). Autoradiographic analysis confirmed that radiotracer accumulation in plaque vessel walls was predominantly localized to macrophage-rich regions, with uptake intensity showing a strong positive correlation with CXCR4 expression levels in corresponding histological sections. Furthermore, [^{68}Ga]Pentixafor PET imaging successfully visualized leukocyte infiltration in post-myocardial infarction hearts and detected acute, diffuse myocardial inflammatory cell infiltration in a murine model of pressure overload-induced heart failure (transverse aortic constriction) [35]. These findings collectively establish [^{68}Ga]Pentixafor as a highly specific, noninvasive PET biomarker for CXCR4 expression in inflammatory lesions, enabling quantitative assessment of spatiotemporal inflammatory cell dynamics, a crucial parameter for monitoring disease progression, therapeutic response, and stratifying patients for anti-inflammatory interventions.

3. Clinical applications of diagnostic radiopharmaceutical [^{68}Ga]Pentixafor

Based on the aforementioned principles, the clinical applications of the diagnostic radiopharmaceutical [^{68}Ga]Pentixafor have diversified significantly, demonstrating substantial value across numerous domains including endocrine disorders, hematologic malignancies, solid tumors, and inflammatory diseases. By enabling non-invasive quantification of CXCR4 receptor expression *in vivo*, this imaging modality provides crucial molecular imaging evidence for precise diagnosis, subtype differentiation, staging, prognostic evaluation, and treatment decision-making in the aforementioned conditions. The following sections will provide a systematic review and detailed discussion of these extensive applications (Table 1).

Table 1. Summary of key clinical studies evaluating [^{68}Ga]Pentixafor PET across disease entities.

Authors	Year	Population	Number of patients	Method	Ref
Herrmann *et al.*	2015	MM	5	Prospective	[31]
Philipp-Abbrederis *et al.*	2015	MM	14	Prospective	[32]
Wang *et al.*	2015	GBM	8	Prospective	[36]
Reiter *et al.*	2015	MI	7	Prospective	[37]
Vag *et al.*	2016	Solid cancers	21	Prospective	[38]
Lapa *et al.*	2016	SCLC	10	Prospective	[39]
Lapa *et al.*	2016	GBM	15	Prospective	[40]
Herhaus *et al.*	2016	AML	10	Prospective	[41]
Bluemel *et al.*	2017	Adrenocortical cancer	30	Prospective	[42]
Lapa *et al.*	2017	MM	35	Prospective	[43]
Derlin *et al.*	2017	UTI	13	Prospective	[44]
Werner *et al.*	2017	Neuroendocrine tumors	12	Prospective	[45]
Herhaus *et al.*	2017	MZL	1	Retrospective	[46]
Lapa *et al.*	2017	Pleural mesothelioma	6	Retrospective	[47]
Bouter *et al.*	2018	Chronic Bone Infection	14	Prospective	[48]
Weiberg *et al.*	2018	AP	51	Retrospective	[49]
Li *et al.*	2018	AP	38	Prospective	[50]
Mayerhoefer *et al.*	2018	CLL	23	Prospective	[51]
Derlin *et al.*	2018	AP	37	Prospective	[52]
Bouter *et al.*	2018	Chronic osteomyelitis	29	Retrospective	[53]
Li *et al.*	2019	AP	72	Prospective	[54]
Luo *et al.*	2019	WM/LPL	17	Prospective	[55]
Breun *et al.*	2019	Vestibular schwannomas	4	Prospective	[56]
Haug *et al.*	2019	MALT	36	Prospective	[57]
Werner *et al.*	2019	Solid tumors	19	Retrospective	[58]
Kircher *et al.*	2020	AP	92	Retrospective	[59]
Pan *et al.*	2020	MM	30	Prospective	[60]
Ding *et al.*	2020	PA	36	Prospective	[61]
Herhaus *et al.*	2020	CNSL	11	Prospective	[62]
Pan *et al.*	2020	Non-Hodgkin lymphoma	27	Retrospective	[63]
Lawal *et al.*	2020	AP	12	Prospective	[64]
Starzer *et al.*	2021	CNSL	7	Prospective	[65]
Mayerhoefer *et al.*	2021	MCL	22	Prospective	[66]
Linde *et al.*	2021	NEC	10	Retrospective	[67]
Duell *et al.*	2021	MZL	22	Retrospective	[68]
Weich *et al.*	2021	NEC	11	Retrospective	[69]
Werner *et al.*	2021	MI	96	Retrospective	[70]
Pan *et al.*	2021	WM/LPL	15	Prospective	[71]
Kuyumcu *et al.*	2021	MM	24	Retrospective	[72]
Lewis *et al.*	2021	Solid cancer	145	Retrospective	[73]
Sarah *et al.*	2022	GBM	7	Retrospective	[74]
Kraus *et al.*	2022	MPNs	12	Retrospective	[75]
Mayerhoefer *et al.*	2022	MALT	26	Prospective	[76]
Chen *et al.*	2022	CNSL	26	Prospective	[77]
Kwon *et al.*	2022	MCL	146	Retrospective	[78]
Buck *et al.*	2022	Solid or hematologic neoplasms	690	Retrospective	[79]
Serfling *et al.*	2022	Solid tumors	90	Retrospective	[80]
Ding *et al.*	2022	Cushing syndrome	31	Retrospective	[81]
Watts *et al.*	2022	Rare lung malignancies	6	Prospective	[82]
Shekhawat *et al.*	2022	MM	34	Prospective	[83]
Lu *et al.*	2022	AP	19	Retrospective	[84]
Kraus *et al.*	2022	MM	87	Retrospective	[85]
Gao *et al.*	2023	PA	50	Prospective	[86]
Watts *et al.*	2023	Lung cancer	94	Prospective	[87]
Mayerhoefer *et al.*	2023	MCL	16	Prospective	[88]
Kosmala *et al.*	2023	MZL	73	Retrospective	[89]
Hartlapp *et al.*	2023	DSRCT	8	Prospective	[90]
Roustaei *et al.*	2023	GBM	24	Prospective	[91]
Zheng *et al.*	2023	PA	120	Prospective	[92]
Zhi *et al.*	2023	HNSCC	12	Retrospective	[93]
Kosmala *et al.*	2024	MZL	32	Retrospective	[94]
Dreher *et al.*	2024	Solid tumors	142	Retrospective	[95]
Jena *et al.*	2024	Soft tissue/bone sarcoma	10	Prospective	[96]
Waheed *et al.*	2024	GBM	19	Prospective	[97]
Yin *et al.*	2024	PA	19	Prospective	[98]
Liu *et al.*	2024	NPC	25	Prospective	[99]
Pan *et al.*	2024	sWM	48	Retrospective	[100]
Schloetelburg *et al.*	2024	ACC	41	Retrospective	[101]
Hadebe *et al.*	2024	HNSCC	23	Prospective	[102]
Chen *et al.*	2024	IBD	5	Retrospective	[17]
Roustaei *et al.*	2024	GBM	26	Prospective	[103]
Kopp *et al.*	2024	SSc-ILD	22	Prospective	[104]
Wu *et al.*	2024	Cushing Disease	43	Retrospective	[105]
Yang *et al.*	2024	MM	19	Prospective	[106]
Zuo *et al.*	2025	PA	61	Retrospective	[107]
Yi *et al.*	2025	PA	37	Prospective	[108]
Zhang *et al.*	2025	PA	208	Retrospective	[109]
Chen *et al.*	2025	CNSL\GBM	124	Retrospective	[110]
Kosmala *et al.*	2025	AP	65	Retrospective	[111]
Li *et al.*	2025	PA	27	Retrospective	[112]
Zheng *et al.*	2025	PA	91	Prospective	[113]
Wang *et al.*	2025	Thymoma	32	Prospective	[114]
Kaur *et al.*	2025	MM	40	Prospective	[115]
Gauthaman *et al.*	2025	MM	13	Prospective	[116]
Hadebe *et al.*	2025	Breast cancer	51	Prospective	[117]
Zheng *et al.*	2025	PA	90	Prospective	[118]
Meng *et al.*	2025	PA	62	Prospective	[119]
Pan *et al.*	2025	MM	25	Retrospective	[120]
Zhoufei *et al.*	2025	PA	25	Prospective	[121]
Shu *et al.*	2025	PA	51	Retrospective	[122]
Zheng et al	2025	PA	197	Prospective	[123]
Diekmann *et al.*	2025	MI	49	Retrospective	[16]

MM: multiple myeloma; GBM: glioblastoma; MI: myocardial infarction; SCLC: small cell lung cancer; AML: acute myeloid leukemia; UTI: urinary tract infection; MZL: marginal zone lymphoma; AP: atherosclerotic plaque; CLL: chronic lymphocytic leukemia; WM/LPL: waldenström macroglobulinemia/lymphoplasmacytic lymphoma; MALT: mucosa-associated lymphoid tissue; PA: primary aldosteronism; CNSL: central nervous system lymphoma; MCL: mantle cell lymphoma; NEC: esophageal cancer; MPNs: myeloproliferative neoplasms; DSRCT: desmoplastic small round cell tumor; NPC: nasopharyngeal carcinoma; sWM: smoldering waldenström macroglobulinemia; ACC: adrenal cortical carcinoma; HNSCC: head and neck squamous cell carcinoma; IBD: inflammatory bowel disease; SSc-ILD: systemic sclerosis-associated interstitial lung disease.

3.1. Endocrine disorders

3.1.1. Primary aldosteronism (PA)

PA represents the most prevalent cause of secondary hypertension, characterized by autonomous excessive aldosterone secretion from the adrenal cortex [124]. Aldosterone-producing adenoma (APA) and idiopathic hyperaldosteronism

(IHA) constitute the two main PA subtypes, accounting for approximately 35% and 60% of cases, respectively. Subtype differentiation, particularly distinguishing between APA and IHA, remains a crucial diagnostic challenge in clinical practice, as it directly influences therapeutic strategy selection (e.g., adrenalectomy versus mineralocorticoid receptor antagonist therapy) and long-term cardiovascular/renal outcomes [125,126].

Recent investigations have revealed that CXCR4 is highly expressed on APA cell membranes and demonstrates a significant positive correlation with aldosterone synthase (CYP11B2) expression levels, while showing minimal expression in non-functioning adrenal adenomas (NFA) [127]. This molecular characteristic establishes CXCR4-specific radiotracer [^{68}Ga]Pentixafor as a convenient, intuitive, and clinically valuable tool for PA subtype classification through targeted molecular imaging. In a prospective study by Jie Ding *et al.*, 36 patients with clinically suspected PA underwent [^{68}Ga]Pentixafor PET/computed tomography (CT) imaging followed by unilateral adrenalectomy [61]. Histopathological and clinical evaluation identified 39 adrenal lesions, including 25 APA, 4 IHA, and 10 NFA. Visual assessment demonstrated that [^{68}Ga]Pentixafor PET/CT achieved 100% sensitivity, 78.6% specificity, and 92.3% accuracy in discriminating APA (Figure 2A-I). The maximum standardized uptake value (SUVmax) in APA lesions (21.34 ± 9.41) significantly exceeded that in non-APA lesions (6.29 ± 2.10; $p < 0.0001$) (Figure 2M-N). These findings establish [^{68}Ga]Pentixafor PET/CT as a reliable non-invasive modality for APA detection (Figure 2O-P). A subsequent study by the same research group demonstrated that [^{68}Ga]Pentixafor PET/CT achieved detection rates exceeding 90% for functional adrenal nodules, with particularly superior performance for nodules ≥ 1 cm in diameter. Owing to its high sensitivity and specificity, this imaging technique shows promise as a valuable tool for surgical decision-making in PA management.

Recent comparative studies have evaluated the diagnostic performance of [^{68}Ga]Pentixafor PET/CT against adrenal venous sampling for subtyping and lateralization of aldosterone hypersecretion. Results indicated over 80% concordance between the two modalities for lateralization in PA patients, including those with bilateral adrenal hyperplasia [108]. In summary, substantial evidence supports the clinical utility of [^{68}Ga]Pentixafor PET/CT across multiple aspects of PA management, including subtype classification, identification of APA/nodules, functional lateralization, therapeutic decision-making, and prognostic evaluation.

3.1.2. Cushing syndrome (CS)

CS represents an endocrine disorder characterized by chronic exposure to excessive cortisol levels, broadly categorized into adrenocorticotropic hormone (ACTH)-dependent (70%-80%) and ACTH-independent (20%-30%) forms [128]. ACTH-dependent CS primarily results from ACTH-producing pituitary adenomas (Cushing's disease) or ectopic ACTH-secreting lesions, while ACTH-independent CS typically stems from autonomous cortisol-secreting adrenal adenomas/carcinomas or, more rarely, bilateral macronodular adrenal hyperplasia [129].

Emerging evidence indicates that CXCR4 is highly expressed in both ACTH-secreting tumors and adrenal cortical lesions. This molecular characteristic has positioned [^{68}Ga]Pentixafor PET imaging as an increasingly valuable tool for differential diagnosis across CS subtypes [130]. In a retrospective analysis by Jie Ding *et al.*, 31 patients (16 with CS and 15 with non-functioning pituitary or adrenal adenomas) underwent [^{68}Ga]Pentixafor PET/CT imaging [81]. Eleven pituitary adenoma patients additionally received [^{18}F]FDG PET/CT for comparison. The study established that using an SUVmax threshold of >8.5 for adrenal lesions, [^{68}Ga]Pentixafor PET/CT achieved 100% sensitivity and 84.9% specificity in diagnosing cortisol-producing adenomas. When applying an SUVmax cutoff of 3.0 for pituitary lesions, the technique demonstrated perfect discrimination (100% sensitivity and specificity) for identifying ACTH-producing pituitary adenomas (Figure 3A-D). Notably, significant correlations were observed between [^{68}Ga]Pentixafor SUVmax and biochemical parameters in pituitary adenomas, including serum ACTH ($r = 0.71$), serum cortisol ($r = 0.80$), and 24-hour urinary free cortisol ($r = 0.53$; all $p < 0.05$). Importantly, no such correlations were found with glucose metabolism parameters, underscoring the specificity of CXCR4 expression in these endocrine tumors (Figure 3E).

A subsequent prospective study involving 43 Cushing's disease patients further demonstrated that [^{68}Ga]Pentixafor PET/magnetic resonance imaging (MRI) outperformed contrast-enhanced MRI alone in localizing ACTH-secreting pituitary adenomas, highlighting the pivotal role of this multimodal molecular imaging approach in preoperative tumor localization for Cushing's disease management [105] (Figure 3F).

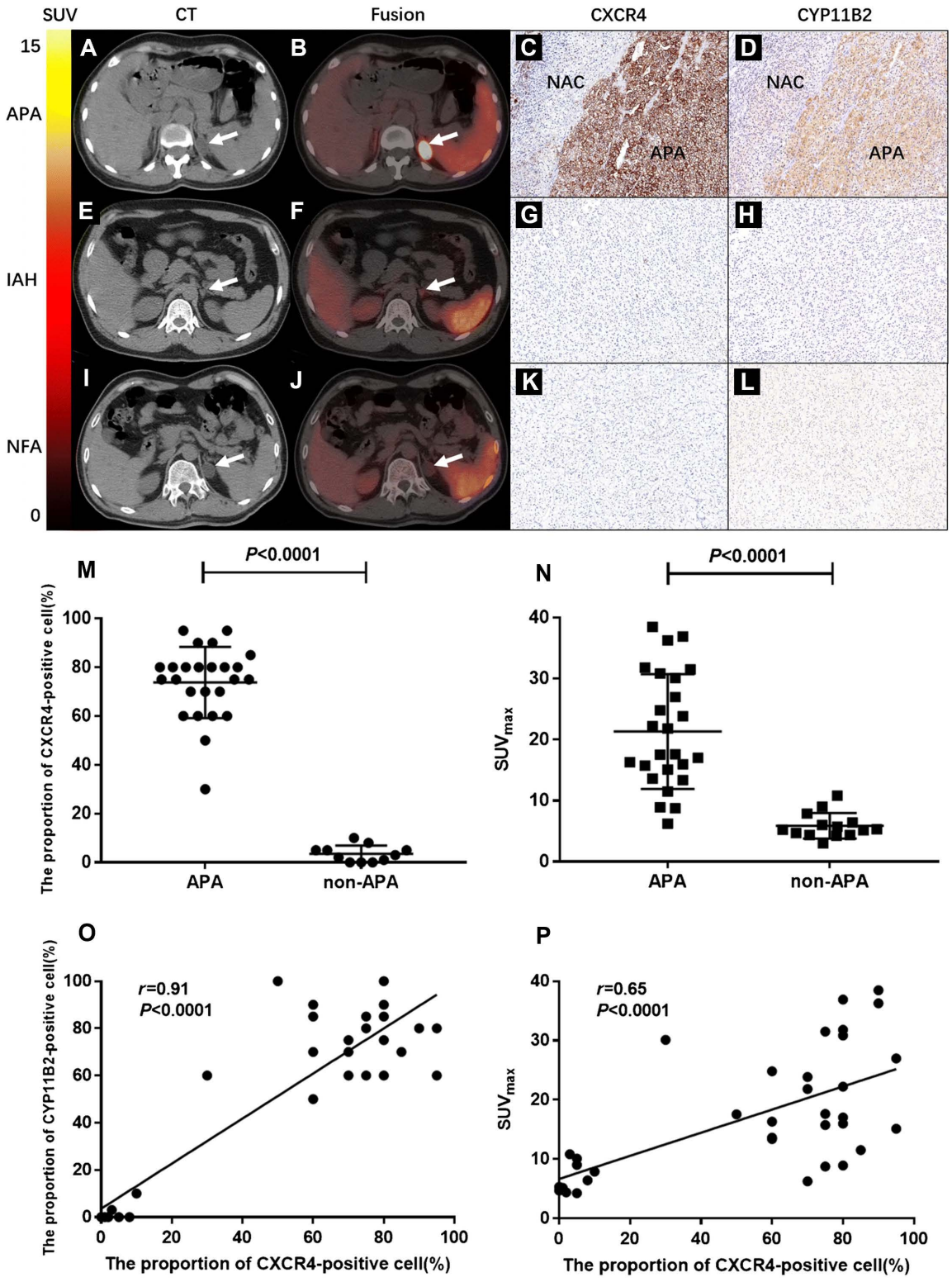

Figure 2. Clinical application of [^{68}Ga]Pentixafor in PA. **(A, B)** Typical [^{68}Ga]Pentixafor PET/CT images of a 44-year-old female. She had fatigue, hypertension, and serum potassium at 2.2 mmol/L. True-positive uptake (SUVmax 36.4, white arrow) was seen in an APA lesion in the left adrenal gland, with strong CXCR4 and CYP11B2 expression (**C, D**; NAC: normal adrenal cortex). CT showed a 2×2.3 cm left adrenal lesion with significant uptake. Post-surgery, her blood pressure and potassium normalized. **(E, F)** Typical images of a 26-year-old male. The test was true-negative in an IAH case. His lowest potassium was 2.7 mmol/L. CT revealed a 1.2 cm left adrenal nodule with slightly increased uptake (SUVmax = 5.3). Immunohistochemistry showed no increased CXCR4 and CYP11B2 expression **(G, H)**. Postoperative hypertension persisted. **(I, J)** Typical images: a 44-year-old male's NFA lesion was true-negative. CT showed a 2.2 cm hypodense left adrenal nodule with no increased uptake (SUVmax = 5.24, white arrow). Histopathology confirmed an adenoma. Immunohistochemistry showed no increased CXCR4 and CYP11B2 expression **(K, L)**. **(M)** The proportion of CXCR4-positive cells (%) was significantly higher in APA than in non-APA lesions ($p < 0.0001$). **(N)** SUVmax values were significantly elevated in APA lesions (21.34 ± 9.41) compared to non-APA lesions (6.29 ± 2.10; $p < 0.0001$). **(O)** Scatter plot demonstrates a significant correlation between CXCR4 expression and CYP11B2 expression levels (%) ($r = 0.91$, $p < 0.0001$). **(P)** A significant correlation was observed between SUVmax of [^{68}Ga]Pentixafor PET and CXCR4 expression levels ($r = 0.65$, $p < 0.0001$). Adapted with permission from [61], copyright © 2020, Springer Nature.

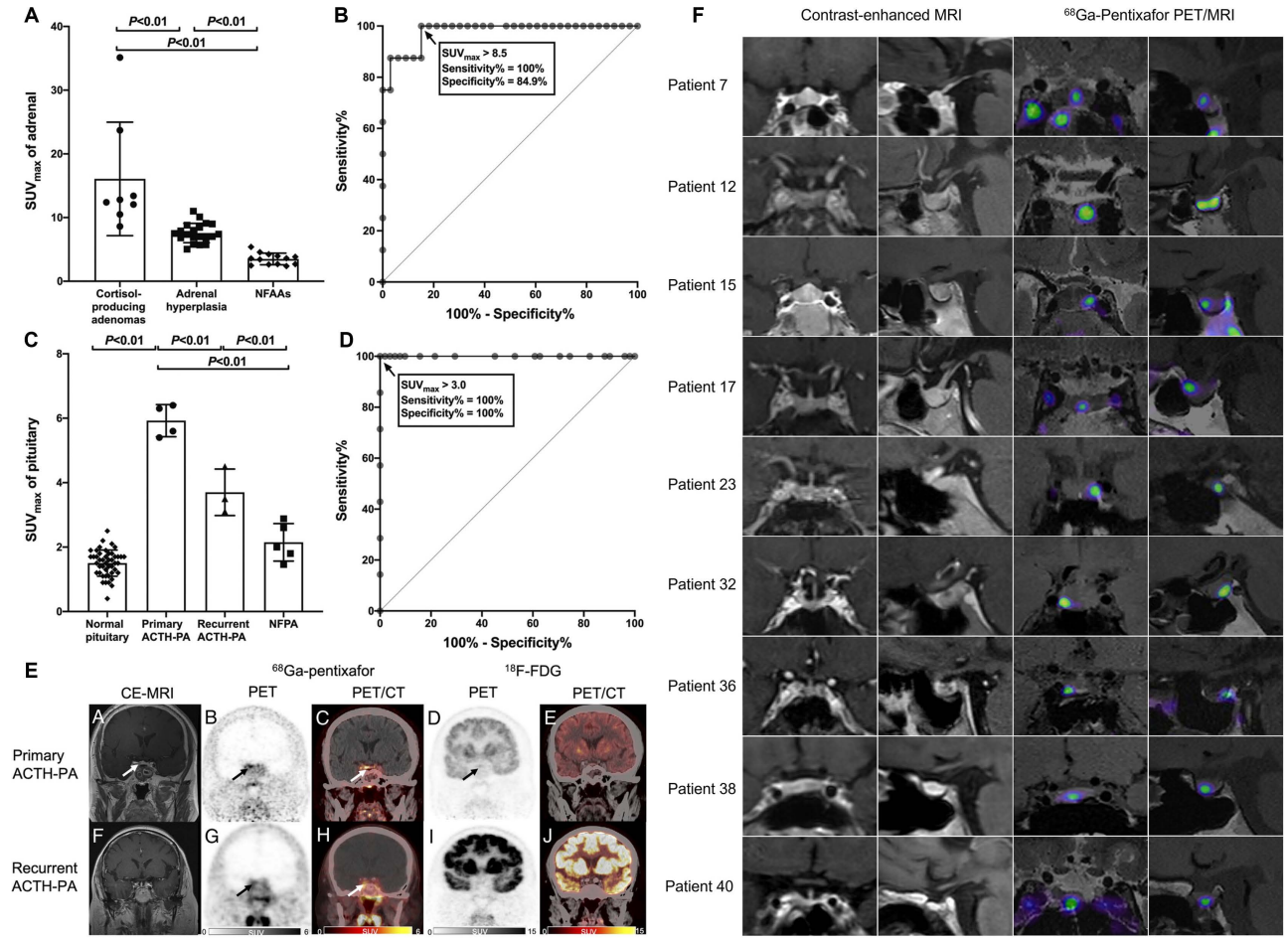

Figure 3. Clinical application of [^{68}Ga]Pentixafor in CS. **(A)** SUVmax comparison of [^{68}Ga]Pentixafor in cortisol-producing adenoma, adrenal hyperplasia, and nonfunctioning adrenal adenoma. **(B)** ROC analysis of [^{68}Ga]Pentixafor SUVmax for discriminating cortisol-producing adenoma from adrenal hyperplasia and nonfunctioning adrenal adenoma. **(C)** SUVmax distribution of [^{68}Ga]Pentixafor across normal pituitary, primary/recurrent ACTH-producing pituitary adenoma, and nonfunctioning pituitary adenoma. **(D)** ROC evaluation of [^{68}Ga]Pentixafor SUVmax for differentiating ACTH-producing pituitary adenoma from nonfunctioning pituitary adenoma and normal pituitary. **(E)** A 41-year-old man with Cushing's disease, pathologically confirmed as a right-sided ACTH-producing pituitary adenoma (5 mm maximum diameter). Contrast-enhanced MRI demonstrated a hypointense microadenoma in the right pituitary wing (arrow). [^{68}Ga]Pentixafor PET/CT coronal PET and fusion images revealed focal uptake (SUVmax 6.3; arrows), while [^{18}F]FDG PET/CT showed only mild diffuse pituitary uptake without distinct foci (arrows). A 41-year-old woman with recurrent right-sided ACTH-producing pituitary adenoma (3 mm maximum diameter). Contrast-enhanced MRI was negative. [^{68}Ga]Pentixafor coronal PET and fusion images demonstrated increased uptake (SUVmax 4.5; arrows), whereas [^{18}F]FDG coronal PET and fusion images showed no abnormal uptake in the pituitary fossa. Adapted with permission from [81], copyright © 2022, Wolters Kluwer. **(F)** Coronal and sagittal contrast-enhanced MRI and corresponding [^{68}Ga]Pentixafor PET/MRI scans in study participants show examples of negative cases (no detected lesion). Adapted with permission from [105], copyright © 2024, Radiological Society of North America.

3.2. Hematological malignancies

3.2.1. MM

MM is characterized by clonal plasma cell proliferation in the bone marrow and overproduction of monoclonal immunoglobulins [131]. CXCR4 activation has been implicated in MM-related bone disease, while the CXCR4/CXCL12 axis promotes plasma cell proliferation. The CXCR4-targeted PET tracer [^{68}Ga]Pentixafor has recently been applied in MM evaluation [31]. Biodistribution studies demonstrate favorable dosimetry for [^{68}Ga]Pentixafor, with an effective dose of 2.3 mSv per 150 MBq administration. The bladder wall receives the highest absorbed dose (12.2 mGy), followed by the spleen (8.1 mGy) and kidneys (5.3 mGy), all lower than corresponding doses from [^{18}F]FDG or ^{68}Ga-labeled somatostatin receptor ligands.

While [^{18}F]FDG PET/CT plays a role in MM workup, its accuracy is limited by false-negative results due to hexokinase-2 expression loss in MM cells, and false-positive findings from fractures, inflammatory changes, or MM-related anemia. A prospective cohort study by Pan *et al.* compared [^{68}Ga]Pentixafor and [^{18}F]FDG PET/CT in newly diagnosed MM patients (n = 30) [60] (Figure 4A-B). [^{68}Ga]Pentixafor demonstrated significantly higher detection rates (93.3% *vs.* 53.3%, p = 0.0005), particularly in cases with diffuse bone marrow patterns (88.2% *vs.* 29.4%, p = 0.002). Quantitative parameters of [^{68}Ga]Pentixafor uptake (TBmUCXCR4, SUVmax, SUVmean) showed significant positive

correlations with end-organ damage severity, disease stage, and tumor burden biomarkers including serum β2-microglobulin, serum free light chains, and 24-hour urinary light chains. These findings underscore the prognostic value of [^{68}Ga]Pentixafor PET/CT in MM, supported by multiple investigations [72,83]. Emerging evidence suggests splenic uptake of [^{68}Ga]Pentixafor may provide prognostic information in pretreated MM patients, comparable to diffusion-weighted MRI [85]. In comparative studies, [^{68}Ga]Pentixafor PET demonstrated superior or equal sensitivity versus [^{18}F]FDG in 63% of cases [43]. [^{68}Ga]Pentixafor PET demonstrates detectable CXCR4 expression across a broad spectrum of MM subtypes, suggesting its potential as a widely applicable imaging biomarker. However, the intensity of uptake (e.g., SUVmax) can vary and has been correlated with disease burden and stage, indicating its quantitative value for risk stratification.

3.2.2. Marginal zone lymphoma (MZL)

MZL, accounting for approximately 7% of indolent non-Hodgkin lymphomas, includes extranodal (EMZL), nodal (NMZL), and splenic (SMZL) subtypes [132]. CXCR4 is physiologically expressed on lymphocytes and has been observed in various T-cell and B-cell neoplasms, including MZL [89]. [^{68}Ga]Pentixafor PET has shown promising results in MZL assessment. A pilot study in treatment-naïve lymphoma patients demonstrated that [^{68}Ga]Pentixafor PET/CT significantly improved MZL detection compared to conventional staging on both per-patient and per-lesion bases ($p < 0.001$) [68] (Figure 4C). Among 18 PET-guided biopsies, 16 confirmed MZL involvement. These findings highlight the utility of [^{68}Ga]Pentixafor PET in primary MZL staging, corroborated by subsequent CXCR4-directed PET/MRI studies [57]. In newly diagnosed MZL patients, [^{68}Ga]Pentixafor identified more disease sites than [^{18}F]FDG across all subtypes [94]. Subgroup analyses further indicated superior diagnostic performance of [^{68}Ga]Pentixafor PET/CT for NMZL and EMZL, suggesting its potential as a preferred novel PET agent for MZL evaluation.

3.2.3. Waldenström macroglobulinemia/ lymphoplasmacytic lymphoma (WM/LPL)

WM/LPL is a rare indolent NHL characterized by bone marrow lymphoplasmacytic infiltration and monoclonal immunoglobulin production [71]. While [^{18}F]FDG PET/CT is valuable for staging FDG-avid nodal lymphomas, its utility in WM/LPL is limited except when assessing aggressive transformation [133]. Studies demonstrate elevated CXCR4 expression in WM/LPL B-cells compared to healthy donors, prompting evaluation of [^{68}Ga]Pentixafor PET/CT in this malignancy [134,135]. A prospective cohort study (n = 17) revealed significantly higher detection rates with [^{68}Ga]Pentixafor versus [^{18}F]FDG PET/CT (100% *vs*. 58.8%; p = 0.023) [55]. For bone marrow involvement, sensitivities were 94.1% and 58.8%, respectively (p = 0.077), while for nodal involvement, [^{68}Ga]Pentixafor demonstrated markedly superior detection (76.5% *vs*. 11.8%; p = 0.003) (Figure 4D-E). Additionally, [^{68}Ga]Pentixafor identified more paraspinal and central nervous system lesions than [^{18}F]FDG.

Further investigation evaluated [^{68}Ga]Pentixafor PET/CT for treatment response assessment in WM/LPL (n = 15) [71]. All patients showed positive baseline [^{68}Ga]Pentixafor PET/CT, compared to only 11 with [^{18}F]FDG PET/CT. Following chemotherapy (overall response rate: 86.7%), [^{68}Ga]Pentixafor PET/CT accurately identified tumor responses in all cases, including new lesions or significantly increased uptake in two progressing patients. In contrast, [^{18}F]FDG PET/CT failed to detect improvement in 6/13 responding patients and missed progression in 1/2 progressing cases. [^{68}Ga]Pentixafor PET/CT outperforms [^{18}F]FDG in uptake intensity, bone marrow involvement visualization, focal lesion detection, and treatment response assessment in WM/LPL.

3.2.4. Mantle cell lymphoma (MCL)

MCL, an aggressive B-cell NHL with approximately 50% 5-year survival, commonly involves lymph nodes, spleen, bone marrow, and gastrointestinal tract [66,78,136,137]. Although [^{18}F]FDG PET is recommended for MCL staging, its uptake can be low to moderate and unreliable for bone marrow assessment [138,139]. A prospective study comparing [^{68}Ga]Pentixafor and [^{18}F]FDG in MCL patients (n = 22) demonstrated significantly higher sensitivity for [^{68}Ga]Pentixafor PET (100% *vs*. 75.2%, $p < 0.001$), with superior SUVs and TBRs [66]. For bone marrow involvement (biopsy-confirmed), [^{68}Ga]Pentixafor SUVmean showed an AUC of 0.92, while for splenic involvement, TBRblood achieved an AUC of 0.81. [^{68}Ga]Pentixafor PET shows promise for non-invasive assessment of bone marrow and splenic involvement in MCL, with significantly higher detection rates and better tumor-to-background contrast than [^{18}F]FDG (Figure 5A-B). In treatment response evaluation, [^{68}Ga]Pentixafor PET detected complete remission earlier and more comprehensively than MRI [88]. At interim assessment, 56.3% of target lesions met CR criteria by [^{68}Ga]Pentixafor PET versus 50.0% by MRI (p = 0.63); at end-of-treatment, corresponding rates were 70.2%

versus 47.4% (p = 0.021), indicating superior performance of [^{68}Ga]Pentixafor PET in evaluating treatment response, particularly upon therapy completion.

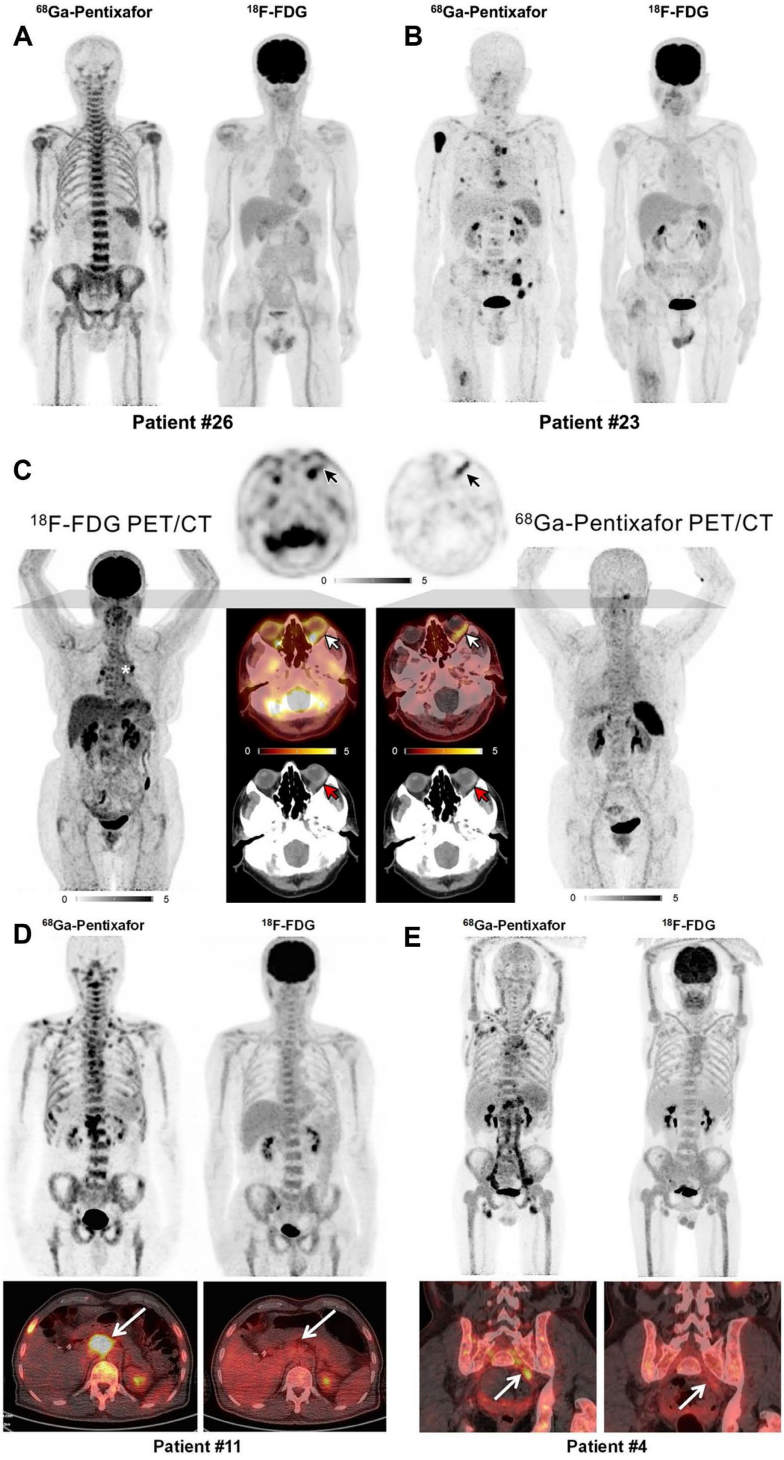

Figure 4. Clinical application of [^{68}Ga]Pentixafor in MM, MZL, and WM/LPL. (A) Patient #26 with IgA-λ MM demonstrating diffuse bone marrow infiltration pattern. Intense [^{68}Ga]Pentixafor uptake in bone marrow with negative [^{18}F]FDG avidity. **(B)** Patient #23 with IgA-λ MM. Multiple bone marrow lesions detected by [^{68}Ga]Pentixafor PET, while [^{18}F]FDG uptake remained negative. Adapted with permission from [60], copyright © 2020, Springer Nature. **(C)** Maximum-intensity-projection images of [^{18}F]FDG and [^{68}Ga]Pentixafor PET in a patient with EMZL. Central axial sections demonstrate orbital lymphoma manifestation with discordant tracer uptake ([^{18}F]FDG-negative, CXCR4-positive), annotated with white (PET/CT), black (PET), and red (CT) arrows. Asterisk indicates intense focal uptake in two hilar lymph nodes; biopsy confirmed sarcoidosis, not MZL. Adapted with permission from [68], copyright © 2021, Society of Nuclear Medicine and Molecular Imaging. **(D)** Patient 11 with WM (IgM λ), ISS-WM score 2 (indeterminate risk). [^{68}Ga]Pentixafor imaging demonstrated intense bone marrow uptake with multifocal lesions and CXCR4-positive lymph nodes (arrows). [^{18}F]FDG activity (score 4) showed homogeneous bone marrow distribution without nodal avidity (arrows). **(E)** Patient 4 with WM (IgM κ) and Bing-Neel syndrome, ISS-WM score 2 (indeterminate risk). Multiple CXCR4-positive lymph nodes were detected in cervical, axillary, hepatoduodenal, retroperitoneal, iliac, and inguinal regions, most undetected by [^{18}F]FDG PET. The involved left iliac nerve root (arrow) was CXCR4-positive but [^{18}F]FDG-negative. Adapted with permission from [55], copyright © 2019, Society of Nuclear Medicine and Molecular Imaging.

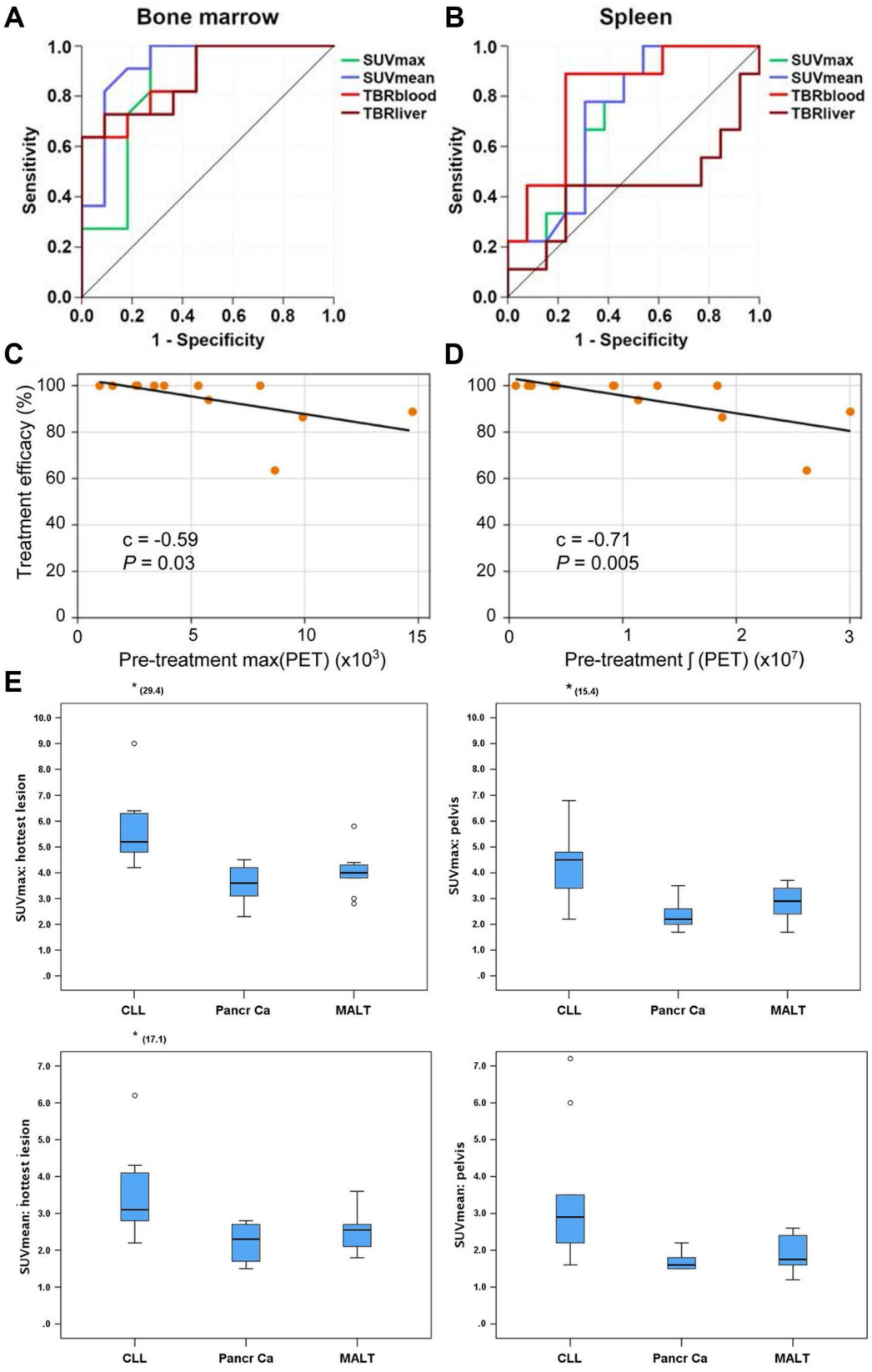

Figure 5. Clinical application of [^{68}Ga]Pentixafor in MCL, CNSL, and CLL. Receiver operating characteristic curves demonstrating the diagnostic performance of [^{68}Ga]Pentixafor PET SUV and TBR for detecting bone marrow **(A)** and splenic involvement **(B)** in MCL patients. Adapted with permission from [66], copyright © 2021, Ivyspring International Publisher. Lesion-based analysis in CNSL patients (14 lymphoma lesions): Correlations between treatment response metric (η) and pretreatment PET parameters—max(PET) **(C)**, and ∫(PET) **(D)**. Scatter plots show Pearson correlation coefficient **(C)** and *P* values, with black line indicating least-squares regression. Adapted with permission from [62], copyright © 2020, Society of Nuclear Medicine and Molecular Imaging. **(E)** Box plots demonstrating differences in SUVmax and SUVmean within pelvic bone marrow and the hottest bone marrow lesions among patients with CLL, pancreatic adenocarcinoma, and MALT lymphoma. Adapted with permission from [51], copyright © 2018, Wolters Kluwer.

3.2.5. Central nervous system lymphoma (CNSL)

A proof-of-concept study evaluated [^{68}Ga]Pentixafor PET in 11 CNSL patients (8 PCNSL, 3 SCNSL) [62]. Quantitative analysis in 7 pretreatment patients revealed excellent tumor-to-brain parenchyma contrast (TBR > 5:1) in all active disease cases. Initial CXCR4 uptake levels significantly correlated with subsequent treatment response to regimens like high-dose methotrexate ($p < 0.05$), with higher CXCR4 expression associated with better remission rates (Figure 5C-D).

3.2.6. Chronic lymphocytic leukemia (CLL)

A prospective study first reported [^{68}Ga]Pentixafor application in CLL, comparing 13 CLL patients with 20 controls (10 pancreatic cancer, 10 mucosa-associated lymphoid tissue, MALT lymphoma) [51] (Figure 5E). [^{68}Ga]Pentixafor uptake was significantly higher in CLL bone marrow than in tumor patients without marrow involvement. Notably, nodal lesion uptake exceeded bone marrow uptake, consistent with previous reports of higher proliferation rates in lymph nodes versus bone marrow in CLL [140].

3.3. Solid tumors

3.3.1. Glioblastoma (GBM)

GBM, representing 45-50% of primary malignant brain tumors in adults, demonstrates poor prognosis due to its infiltrative growth pattern, frequent recurrence, and therapeutic resistance [141,142]. CXCR4 overexpression correlates with tumor angiogenesis and adverse outcomes in GBM [143,144]. The clinical application of CXCR4-targeted [^{68}Ga]Pentixafor PET/CT has been increasingly explored in this context.

A preoperative imaging study enrolled 15 patients with suspected primary or recurrent GBM [40]. [^{68}Ga]Pentixafor PET/CT demonstrated visual positivity in 13/15 cases, with SUVmean 3.0 ± 1.5 and SUVmax 3.9 ± 2.0. While absolute uptake values were lower than those of [^{18}F]FET PET/CT (SUVmean 4.4 ± 2.0, SUVmax 5.3 ± 2.3), [^{68}Ga]Pentixafor achieved significantly higher TBRs for both SUVmean (154.0 ± 90.7 *vs*. 4.1 ± 1.3) and SUVmax (70.3 ± 44.0 *vs*. 3.8 ± 1.2, $p < 0.01$). Histopathological analysis confirmed concordance between high [^{68}Ga]Pentixafor uptake regions and CXCR4 expression, establishing the feasibility of non-invasive CXCR4 imaging in GBM (Figure 6A). Analysis of the GEO dataset GSE16011 (n = 284) revealed negligible CXCR4 mRNA expression in healthy brain tissue versus significant inter- and intra-tumoral heterogeneity in GBM, supporting [^{68}Ga]Pentixafor's potential for patient stratification in CXCR4-directed therapies [74].

In treatment response assessment, Waheed *et al.* performed serial [^{68}Ga]Pentixafor PET/CT in 10 GBM patients undergoing radiochemotherapy (R-CT) [97]. Baseline mean SUVmax (4.6 ± 2.1) showed no significant difference from post-R-CT values (4.4 ± 1.6). However, during 6-month follow-up, patients with stable disease (n = 4) exhibited significantly lower SUVmax and tumor/blood ratios (3.70 ± 0.90, 2.64 ± 1.35) compared to baseline (4.40 ± 2.8, 2.91 ± 0.93), while progressing patients (n = 6) demonstrated significantly elevated parameters versus both baseline and stable disease groups ($p < 0.05$) (Figure 6B-I). These findings suggest [^{68}Ga]Pentixafor's potential for R-CT response assessment, though larger multicenter trials are warranted for validation.

3.3.2. Head and neck squamous cell carcinoma (HNSCC)

HNSCC, comprising over 90% of head and neck malignancies, ranks as the sixth most common cancer globally with poor overall survival [145,146]. While [^{18}F]FDG remains the primary radiotracer for HNSCC staging, its limitations include poor detection of small tumors and difficulty distinguishing recurrence from post-treatment changes.

Comparative studies by Zhi *et al.* demonstrated lower detection rates for [^{68}Ga]Pentixafor versus [^{18}F]FDG in HNSCC, particularly for primary tumors [93] (Figure 7A-B). Immunohistochemistry revealed variable CXCR4 expression in both primary tumors and lymph nodes, with no significant correlation between *in vitro* CXCR4 upregulation and [^{68}Ga]Pentixafor parameters (TBR: $r = 0.33$, $p = 0.39$; SUVmax: $r = 0.44$, $p = 0.2$). Notably, CXCR4 expression in germinal center centroblasts sometimes exceeded tumor cell expression, suggesting inflammatory microenvironment contributions [147]. The limited performance of [^{68}Ga]Pentixafor may be attributed to reactive lymphoid hyperplasia and immune cell infiltration within the tumor microenvironment [148].

Subtype analysis revealed more pronounced tracer accumulation in nasopharyngeal carcinoma (NPC) compared to oropharyngeal and oral cavity malignancies [102]. A prospective study demonstrated comparable detection rates between [^{68}Ga]Pentixafor and [^{18}F]FDG PET/CT for primary nasopharyngeal tumors and metastatic cervical lymph nodes [99] (Figure 7C). A distinct advantage of [^{68}Ga]Pentixafor is the absence of physiological uptake in brown adipose tissue, eliminating potential imaging interference in cervical regions.

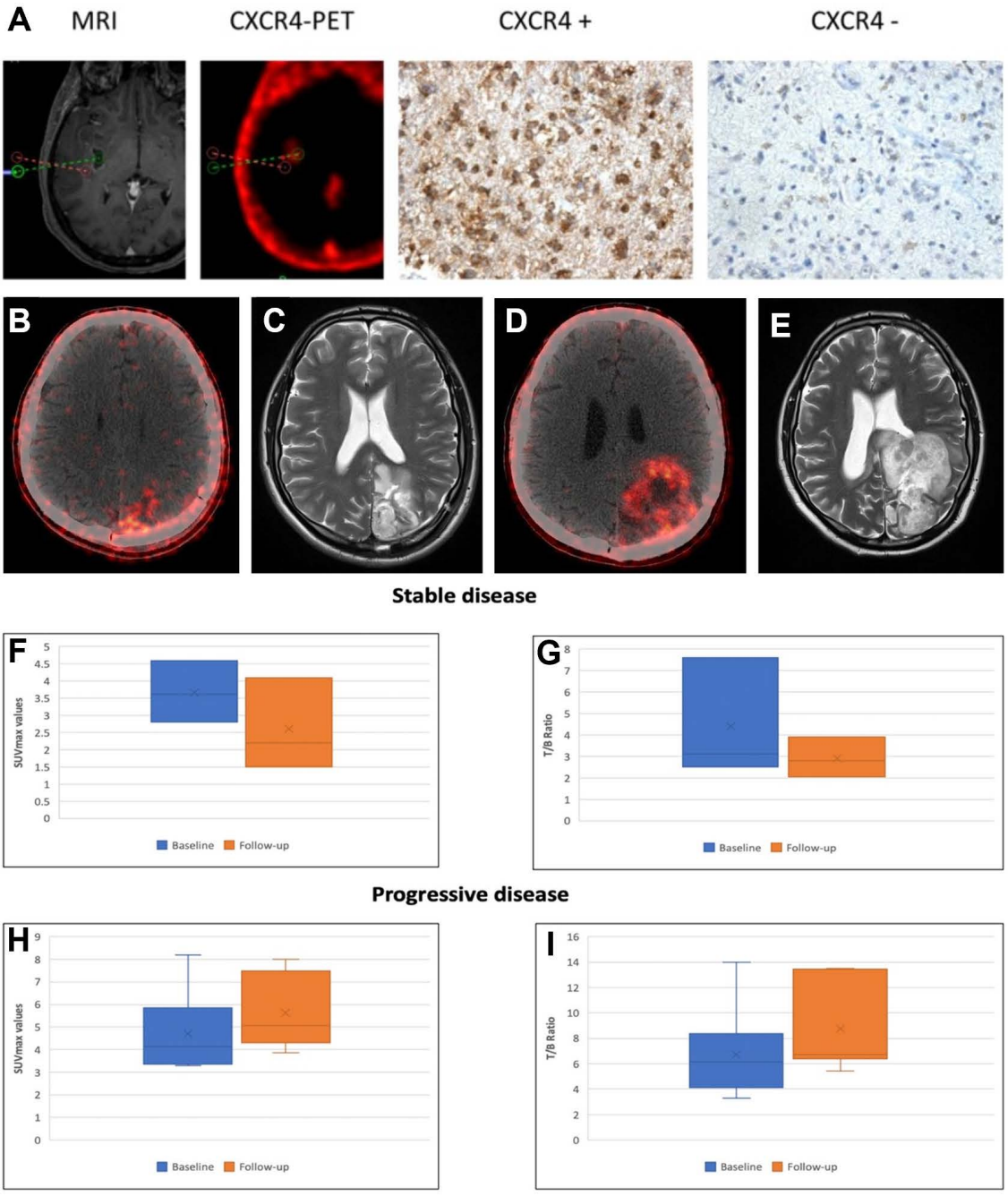

Figure 6. Clinical application of [^{68}Ga]Pentixafor in GBM. (A) CXCR4 Expression in PET-Positive *vs*. PET-Negative Tumor Samples (assessed by [^{68}Ga]Pentixafor PET). Representative immunohistochemical staining showing CXCR4 expression in [^{68}Ga]Pentixafor-negative (red dotted area; [^{18}F]FET-positive) and positive (green) tumor regions. Integrated neuronavigation with [^{68}Ga]Pentixafor PET/CT and MP-RAGE MRI guided targeted biopsy. H&E nuclear staining. Magnification: 200×. Adapted with permission from [40], copyright © 2016, Ivyspring International Publisher. Axial fused [^{68}Ga]Pentixafor PET/CT images in a 31-year-old male GBM patient post-craniotomy demonstrate tracer uptake (SUVmax = 8.18, T/B ratio = 6.5) in a 2.0 cm left parietal lobe lesion **(B)**. 3-month post-R-CT follow-up [^{68}Ga]Pentixafor PET/CT **(D)** indicates disease progression (SUVmax = 7.3, T/B ratio = 13.5). Corresponding T2-weighted axial MRI at baseline **(C)** and 3-month post-treatment **(E)** confirm disease progression with increased tumor size. Box-and-whisker plots showing decreased SUVmax **(F)** and T/B ratios **(G)** in patients with stable disease, and increased SUVmax **(H)** and T/B ratios **(I)** in those with progressive disease. Adapted with permission from [97], copyright © 2024, Wolters Kluwer.

3.3.3. Lung malignancies

SCLC, representing 13-15% of lung cancers, demonstrates early hematogenous spread to brain, liver, and bones, with 60-70% of patients presenting with extensive-stage disease at diagnosis [149,150]. Initial studies documented non-invasive CXCR4 assessment in SCLC using [^{68}Ga]Pentixafor PET, demonstrating positivity in 8/10 patients with superior lesion detection compared to [^{68}Ga]DOTATOC PET and significantly higher TBRs [39]. While [^{18}F]FDG detected two cases missed by [^{68}Ga]Pentixafor, the latter identified equal or greater numbers of lesions in remaining patients, supporting

its utility for detecting CXCR4 expression and screening patients for targeted therapies.

In non-small cell lung cancer (NSCLC), [^{68}Ga]Pentixafor PET/CT demonstrated remarkable clarity in detecting brain metastases, addressing a known limitation of [^{18}F]FDG PET [151]. Comprehensive analysis across lung cancer subtypes revealed significantly higher [^{68}Ga]Pentixafor uptake in SCLC (mean SUVmax = 10.3 ± 5.0) compared to NSCLC (n = 75) and pulmonary neuroendocrine neoplasms (n = 5, p = 0.005) [87]. Among NSCLC subtypes, adenocarcinoma (n = 16) showed significantly higher uptake (mean SUVmax = 8.0 ± 1.9) than squamous cell carcinoma (n=54; 6.2 ± 2.1) and NOS subtypes (n = 5; 5.8 ± 1.5, p = 0.003). [^{68}Ga]Pentixafor PET/CT demonstrated good sensitivity (85.7%) and specificity (78.1%) in differentiating SCLC from NSCLC at ROC cutoff SUVmax 7.2, and similar performance (sensitivity 87.5%, specificity 71.4%) in distinguishing adenocarcinoma from squamous cell carcinoma at cutoff SUVmax 6.7.

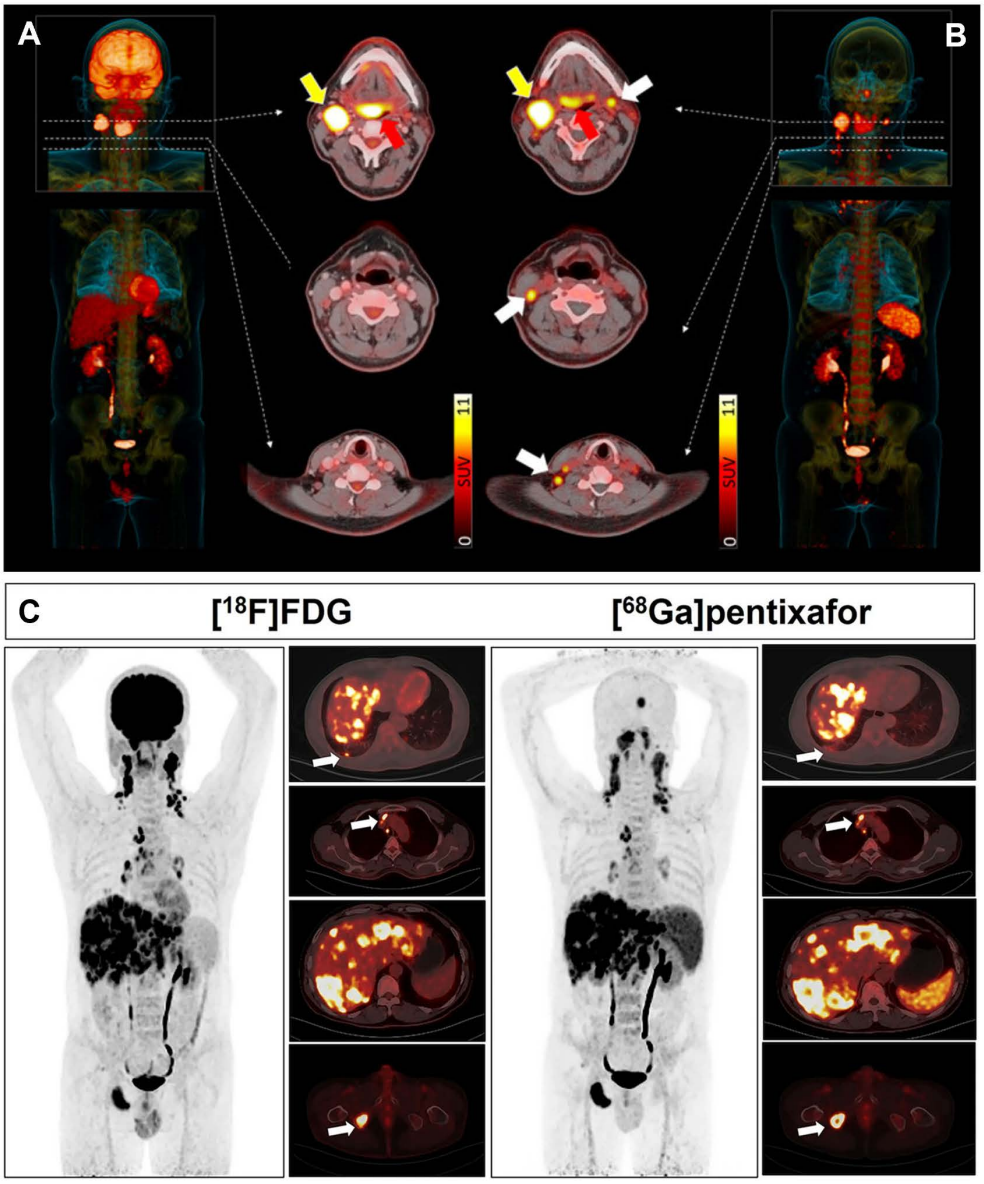

Figure 7. Clinical application of [^{68}Ga]Pentixafor in HNSCC. (A, B) Patient with tongue base carcinoma (red arrow). [^{18}F]FDG PET/CT shows a histologically confirmed right-sided lymph node metastasis (yellow arrow). Additional cervical lymph node findings (white arrows) were exclusively detected by [^{68}Ga]Pentixafor PET/CT. Left: [^{18}F]FDG PET/CT MIP. Right: [^{68}Ga]Pentixafor PET/CT MIP. Middle: Three transaxial PET/CT slices for [^{18}F]FDG (left) and [^{68}Ga]Pentixafor (right). While the primary tumor showed higher [^{18}F]FDG than [^{68}Ga]Pentixafor uptake (red arrow), [^{18}F]FDG identified a single metastatic LN at the right jaw angle (yellow arrow), histologically confirmed. [^{68}Ga]Pentixafor PET/CT detected multiple CXCR4-positive LNs along bilateral cervical neurovascular sheaths, initially suspected as metastases. Histology confirmed these LNs (white arrows) represented inflammatory/reactive changes with lymphofollicular hyperplasia. Adapted with permission from [93], copyright © 2023, e-Century Publishing Corporation. **(C)** Comparative [^{18}F]FDG and [^{68}Ga]Pentixafor imaging in a 49-year-old treatment-naïve male with NPC and multiorgan metastases. Both PET/CT scans demonstrate abnormal tracer uptake in: lung (arrow; SUVmax 5.20 vs 3.00), mediastinal lymph nodes (arrow; SUVmax 9.75 vs 7.35), liver (SUVmax 11.00 vs 10.01), and bone (arrow; SUVmax 8.48 vs 11.57). Adapted with permission from [99], copyright © 2024, Springer Nature.

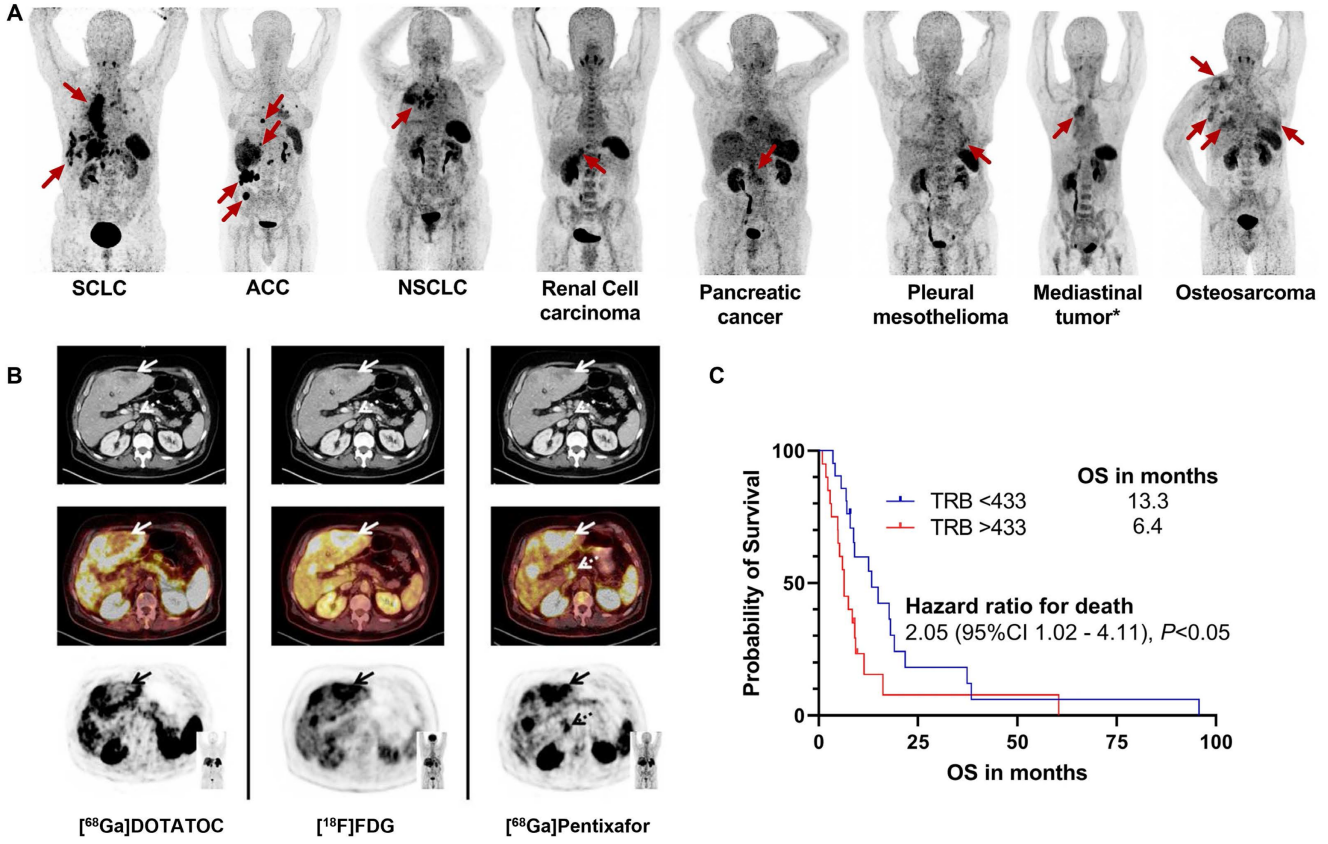

Figure 8. Clinical application of [^{68}Ga]Pentixafor in other cancer types. (A) CXCR4-targeted PET/CT with [^{68}Ga]Pentixafor across solid tumor entities. Maximum intensity projections are displayed. Red arrows indicate CXCR4-positive tumor lesions. ACC: adrenocortical carcinoma; NEN: neuroendocrine neoplasia; NSCLC: non-small cell lung carcinoma; SCLC: small cell lung carcinoma. *Not otherwise specified. Adapted with permission from [95], copyright © 2024, Springer Nature. **(B)** Tumor heterogeneity in a G3 gastric NET with liver metastases (Ki67: 90%). Hypermetabolic liver lesions show SSTR loss and CXCR4 upregulation (solid arrows; [^{68}Ga]Pentixafor SUVmax 10.3 *vs* [^{68}Ga]DOTATOC SUVmax 3.8). [^{68}Ga]Pentixafor exclusively detected a suspicious celiac lymph node (dotted arrow), providing additional staging information. All transaxial PET/(CT) images displayed at window level 0-5.5. Adapted with permission from [45], copyright © 2017, Ivyspring International Publisher. **(C)** Kaplan-Meier analysis of overall survival by tumor receptor binding (TRB) on [^{68}Ga]Pentixafor PET. Elevated TRB (stratified by median value) correlates with reduced survival. Adapted with permission from [101], copyright © 2024, Springer Nature.

3.3.4. Other cancer types

[^{68}Ga]Pentixafor PET has been extensively evaluated in various malignancies including pancreatic, prostate, breast, hepatocellular carcinoma, sarcomas, and cancers of unknown primary [38]. A comprehensive study involving 142 patients with 23 different histologically confirmed solid tumors undergoing 152 [^{68}Ga]Pentixafor PET/CT scans demonstrated exceptional image contrast with median TBR >4 across all tumor types compared to normal physiological background [95] (Figure 8A). These data not only confirm the widespread overexpression of CXCR4 across various solid tumors but, more importantly, their high-contrast imaging characteristics provide crucial visual evidence for accurately identifying CXCR4-positive lesions and guiding subsequent targeted therapies.

Notably, substantial variations in [^{68}Ga]Pentixafor positivity rates exist among different tumor types, suggesting that transcriptomic profiling or whole-cell protein measurements may not fully reflect actual cell surface CXCR4 expression [1,152]. This discrepancy may stem from differences in receptor internalization and recycling regulated by the tumor microenvironment, variations in the activation status of downstream signaling pathways, or uneven subclonal distribution due to tumor heterogeneity. Therefore, *in vivo* PET imaging may hold greater clinical relevance than *ex vivo* molecular assays in assessing functional, targetable CXCR4 expression. In gastrointestinal and pancreatic neuroendocrine tumors (GEP-NETs), [^{68}Ga]Pentixafor positivity correlated with high proliferative activity (Ki67 index ≥ 85%), while well-differentiated tumors showed minimal receptor expression [45] (Figure 8B). All CXCR4-positive subjects demonstrated high [^{18}F]FDG uptake but relatively low or absent somatostatin receptor expression as evaluated by [^{68}Ga]DOTATOC, indicating an inverse correlation between CXCR4 and SSTR2 expression with increasing tumor grade in G1-G3 neuroendocrine

tumors [153]. This finding carries significant implications for subtyping and treatment guidance. CXCR4 imaging may help identify more aggressive subsets of neuroendocrine tumors that are less responsive to traditional somatostatin analog therapies, thereby steering treatment toward more intensive strategies.

In adrenal cortical carcinoma (ACC), *in vitro* experiments confirmed high CXCR4 expression at lesion sites. [^{68}Ga]Pentixafor PET TBR independently correlated with shorter overall survival in metastasized ACC patients, providing valuable prognostic information for disease progression monitoring and treatment guidance [101] (Figure 8C). This suggests that CXCR4 imaging is not merely a diagnostic tool but may also serve as a biomarker for predicting aggressive tumor biological behavior and patient prognosis. Future research could further explore incorporating quantitative PET parameters (such as SUVmax, TBR) into risk stratification models to optimize therapeutic decision-making.

While these findings are encouraging, it is essential to recognize the challenges before CXCR4-targeted theranostics can be widely applied in solid tumors. These include intra- and inter-tumoral heterogeneity, physiological uptake of tracers in non-target tissues, and the complex biological barriers involved in translating high diagnostic sensitivity into effective therapeutic responses. Future research should focus on identifying patient subpopulations most likely to benefit from CXCR4-targeted therapies and exploring combination strategies with other treatment modalities, such as immunotherapy.

3.4. Inflammatory diseases

The chemokine receptor CXCR4 demonstrates significant expression across various inflammatory pathologies, playing crucial roles in immune cell recruitment and chronic inflammation maintenance [30,154]. In atherosclerosis, the CXCL12/CXCR4 axis exerts pro-atherogenic, pro-thrombotic, and plaque-destabilizing effects. CXCR4 expression is observed not only in monocytes migrating to arterial lesions, differentiated macrophages, and lymphocytes, but also in smooth muscle progenitor cells and endothelial progenitor cells participating in plaque evolution. Accumulating evidence from both experimental and clinical studies supports the utility of [^{68}Ga]Pentixafor PET for detecting CXCR4 expression levels in vascular walls [30,49].

In a prospective study by Xiang Li *et al.*, 72 lymphoma patients underwent whole-body [^{68}Ga]Pentixafor PET/MRI with dedicated T2-weighted carotid sequencing [54] (Figure 9A). Consistent with previous investigations, eccentric atherosclerotic lesions demonstrated significantly higher [^{68}Ga]Pentixafor uptake compared to non-stenotic lesions, indicating elevated CXCR4 expression [30,49]. Malte Kircher *et al.* directly compared [^{68}Ga]Pentixafor PET/CT and [^{18}F]FDG PET/CT for atherosclerosis imaging in large arterial walls [59]. [^{68}Ga]Pentixafor PET detected more lesions (n = 290; TBR ≥ 1.6, p < 0.01) with significantly higher uptake values (1.8 ± 0.5 *vs*. 1.4 ± 0.4; p < 0.01) than [^{18}F]FDG PET (Figure 9B-C). However, only weak correlation was observed between the uptake patterns of these two tracers, necessitating further investigation to elucidate the biological mechanisms underlying CXCR4 positivity.

In AMI, CXCR4 facilitates stem cell and progenitor cell recruitment to infarct zones while regulating post-infarction inflammatory responses and resolution. The inaugural *in vivo* study of CXCR4 imaging in human hearts following myocardial infarction demonstrated enhanced chemokine expression in 3 of 7 patients with (sub)acute infarction [155] (Figure 9D-F). Tracer uptake in infarcted myocardium was two-fold higher than in remote myocardium, with negative results in the remaining four patients. Notably, troponin and creatine kinase levels were elevated in PET-positive compared to PET-negative patients, suggesting that hypoxia-induced myocardial damage may trigger CXCR4 upregulation to initiate healing processes. Subsequent research revealed time-dependent [^{68}Ga]Pentixafor uptake in infarcted myocardium, showing linear decline before day 13 post-ischemia, indicating infiltrating inflammatory cells as the primary cellular source of tracer uptake [37,156].

Beyond atherosclerosis and myocardial infarction, CXCR4-targeted [^{68}Ga]Pentixafor PET has been applied for non-invasive detection and localization of various inflammatory conditions including urinary tract infections, chronic skeletal infections, osteomyelitis, inflammatory bowel disease, and systemic sclerosis-associated interstitial lung disease [17,44,48,53,104]. For chronic skeletal infections, a retrospective analysis of 14 patients undergoing [^{68}Ga]Pentixafor PET/CT demonstrated positive results in 9 cases, with target-to-background ratios ranging from 5.1 to 15 (mean 8.7) [48] (Figure 9G-I). Pathological, bacteriological, or clinical confirmation identified 8 true positives among these 9 cases, with one false positive where MRI revealed vertebral necrotic plasmacytoma rather than spondylitis. These findings indicate [^{68}Ga]Pentixafor PET/CT's suitability for diagnosing chronic skeletal infections.

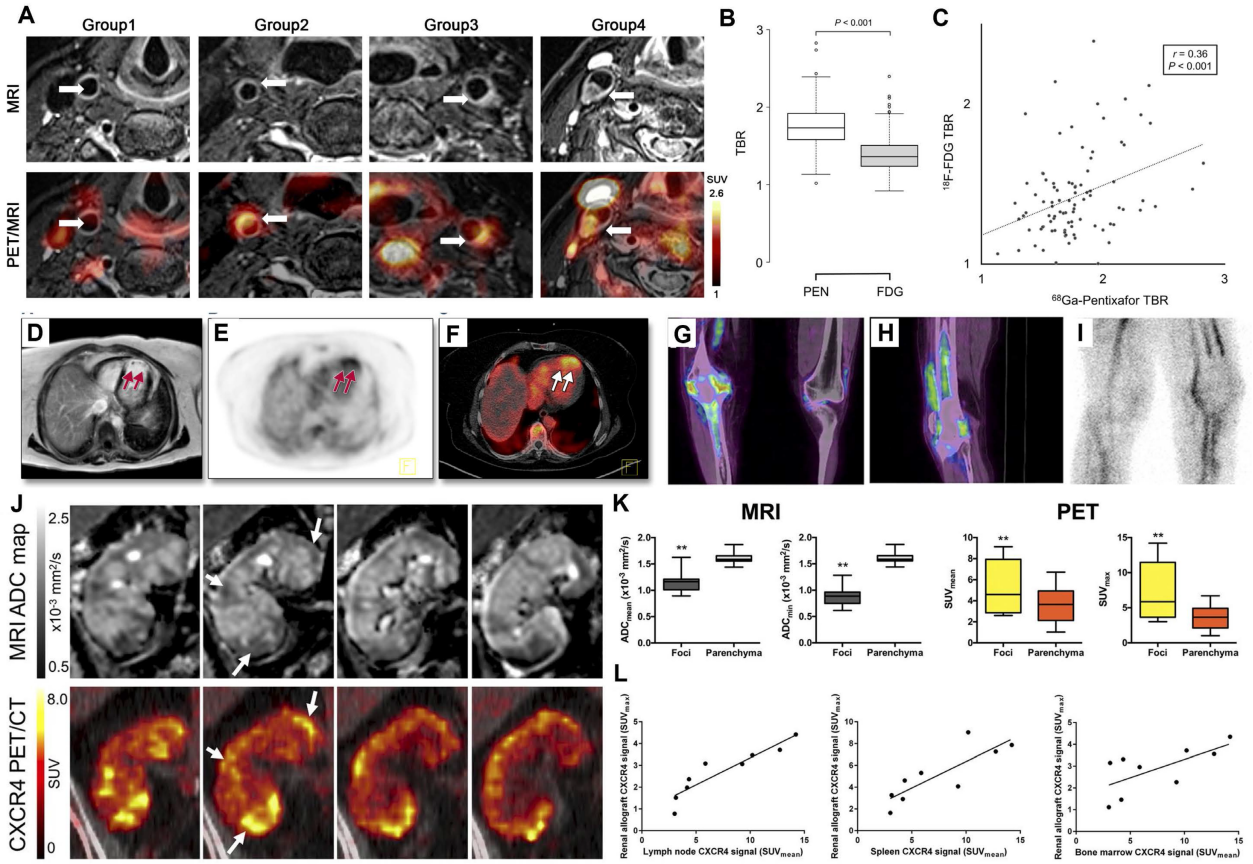

Figure 9. Clinical application of [^{68}Ga]Pentixafor in inflammatory diseases. (A) Representative transaxial [^{68}Ga]Pentixafor PET/MRI images of carotid lesions across study groups. Focal tracer uptake is seen in mildly atherosclerotic carotids with slight eccentric thickening (Group 1), and in moderately (Group 3) to severely (Group 4) atherosclerotic carotids with marked eccentric thickening. No significant uptake is observed in control carotids without eccentric thickening (Group 1). Arrows indicate arterial regions of interest. Adapted with permission from [54], copyright © 2019, Springer Nature. Lesion-based comparison of [^{68}Ga]Pentixafor and [^{18}F]FDG uptake in atherosclerotic plaques. Box plot **(B)** and scatter plot **(C)** demonstrate correlation between [^{18}F]FDG and [^{68}Ga]Pentixafor (PEN) uptake measured by TBR. Adapted with permission from [59], copyright © 2020, Society of Nuclear Medicine and Molecular Imaging. Increased [^{68}Ga]Pentixafor uptake in acute myocardial infarction involving the left anterior descending artery. Axial views of **(D)** contrast-enhanced multishot IR-TFE CMR, **(E)** CXCR4-targeted PET, and **(F)** fused PET/CT demonstrate apical tracer uptake colocalizing with myocardial damage on CMR (arrows). Adapted with permission from [155], copyright © 2015, ELSEVIER. Definite osteomyelitis in a 52-year-old patient with elevated CRP 5 months after total knee arthroplasty removal and spacer implantation. Coronal **(G)** and sagittal **(H)** [^{68}Ga]Pentixafor PET/CT show increased tracer uptake in tibial and femoral bones (including bone marrow). **(I)** Sagittal [^{99m}Tc]besilesomab scintigraphy at 4 h demonstrates osteitis without bone marrow uptake. Adapted with permission from [48], copyright © 2018, Society of Nuclear Medicine and Molecular Imaging. **(J)** Representative MR and PET images of acute renal allograft infection. ADC maps (left, coronal views) demonstrate reduced values colocalizing with CXCR4-upregulated foci on [^{68}Ga]Pentixafor PET (right, arrows). T2-weighted MRI and MIP PET provide anatomical orientation. The renal allograft is located in the right lower abdomen. Spleen shows physiological CXCR4 expression due to leukocyte abundance. **(K)** Box plots of MRI ADC values and [^{68}Ga]Pentixafor SUV in CXCR4-positive foci versus unaffected allograft parenchyma (n = 9). **(L)** CXCR4$^+$ leukocyte accumulation coincides with bone marrow and lymphoid organ upregulation, indicating systemic inflammatory response. Boxes represent IQR (median line); whiskers show range. $^{**}p < 0.01$. Adapted with permission from [44], copyright © 2017, Society of Nuclear Medicine and Molecular Imaging.

Thorsten Derlin *et al.* compared spatial distribution and intensity of CXCR4 upregulation (via [^{68}Ga]Pentixafor PET SUVs) with diffusion restriction (via MRI apparent diffusion coefficients) in 13 kidney transplant recipients with complicated urinary tract infections [44] (Figure 9J-L). PET-identified CXCR4 upregulation regions correlated with leukocyte infiltration areas showing increased cell density on MRI, supporting [^{68}Ga]Pentixafor PET's potential for non-invasive leukocyte detection in renal allografts.

4. Clinical applications of therapeutic radiopharmaceutical [^{177}Lu]/[^{90}Y]Pentixather

Radiotheranostics represents an innovative and rapidly advancing paradigm in precision medicine that integrates diagnostic imaging with targeted radiotherapy [157,158]. This approach fundamentally operates on the principle of delivering the right radiopharmaceutical to the right patient, optimizing therapeutic efficacy while minimizing adverse effects [159,160]. By utilizing diagnostic imaging to identify suitable candidates and guide treatment planning, radiotheranostics enables precise lesion targeting and personalized dose delivery [161,162]. This strategy proves particularly valuable for patients with disseminated or inoperable metastatic malignancies, offering new avenues for disease management. Established clinical examples include [^{68}Ga]/[^{177}Lu]DOTATATE for neuroendocrine tumors and [^{68}Ga]/[^{177}Lu]PSMA for prostate cancer [163–166]. Building upon promising diagnostic results with the

CXCR4-targeted radioligand [^{68}Ga]Pentixafor, therapeutic analogs [^{177}Lu]/[^{90}Y]Pentixather have been developed, forming a novel theranostic pair for CXCR4-directed endoradiotherapy [105,119,123] (Table 2).

4.1. Clinical application status of [^{177}Lu]/[^{90}Y]Pentixather in various malignancies

The inaugural clinical application of [^{177}Lu]/[^{90}Y]Pentixather focused on CXCR4-targeted radionuclide therapy in advanced MM [20] (Figure 10A-B). Initial studies involving high-risk MM patients demonstrated promising initial response rates with favorable safety and tolerability profiles. However, these early outcomes did not translate into significant overall survival prolongation. Biokinetic and dosimetric analyses by Heribert *et al.* revealed median absorbed doses of 0.91 Gy (range: 0.38 - 3.47 Gy) to kidneys and 0.47 Gy (range: 0.14 - 2.33 Gy) to bone marrow per GBq of [^{177}Lu]Pentixather, while [^{90}Y]Pentixather delivered corresponding doses of 3.75 Gy (range: 1.48 - 12.2 Gy) and 1.60 Gy (range: 0.27 - 4.45 Gy) per GBq [170] (Figure 10C-D). Tumor and extramedullary lesions received estimated doses ranging from 1.5 to 18.2 Gy/GBq of [^{90}Y]Pentixather. For hematologic malignancies, these calculated absorbed doses to bone marrow and extramedullary lesions may provide valuable adjunctive therapy alongside high-dose chemotherapy in stem cell transplantation protocols.

Beyond MM, CXCR4-targeted radionuclide therapy has shown potential across various hematologic and solid malignancies [90,171,172]. In AML, [^{177}Lu]Pentixather has been investigated as a conditioning regimen before hematopoietic stem cell transplantation, demonstrating efficient leukemia cell reduction while exhibiting acceptable toxicity profiles [172]. Preliminary results indicate successful bone marrow targeting with minimal damage to vital organs, suggesting potential for improving transplantation outcomes. Due to high physiological CXCR4 expression in the bone marrow, CXCR4-targeted radionuclide therapy is associated with severe, on-target marrow toxicity that is often intentional in conditioning settings. Consequently, most clinical Pentixather-based TRT protocols have incorporated or required subsequent hematopoietic stem cell transplantation, substantially limiting broader clinical applicability.

For solid tumors, clinical experience remains limited but promising. Case reports have documented [^{177}Lu]Pentixather application in CXCR4-positive GBM, pancreatic cancer, triple-negative breast cancer, and neuroendocrine cancer, where conventional therapies had been exhausted [173]. These reports describe disease stabilization and symptomatic improvement in selected patients, particularly those with high CXCR4 expression confirmed by [^{68}Ga]Pentixafor PET imaging. The therapy appears most beneficial for patients with limited tumor burden and predominantly osseous metastases, where favorable biodistribution patterns enhance therapeutic efficacy.

Several challenges require addressing for optimal clinical implementation. The heterogeneous expression of CXCR4 within tumors may lead to incomplete lesion targeting, while potential hematological toxicity necessitates careful patient selection and dose optimization [85,174]. Current research focuses on combination strategies with conventional chemotherapy, immunotherapy, and other targeted agents to enhance treatment efficacy [172]. Additionally, the development of alpha-emitting CXCR4-targeted radiopharmaceuticals (e.g., [^{225}Ac]Pentixather) represents an emerging approach to improve therapeutic index, particularly for micrometastatic disease.

Table 2. Summary of key clinical studies evaluating [^{177}Lu]/[^{90}Y]Pentixather across disease entities.

Authors	Year	Population	Number of patients	Radiopharmaceutical	Ref
Herrmann *et al.*	2016	MM	3	[^{177}Lu]/[^{90}Y]Pentixather	[20]
Habringer *et al.*	2018	AML	3	[^{177}Lu]Pentixather	[33]
Lapa *et al.*	2018	MM	3	[^{177}Lu]Pentixather	[167]
Maurer *et al.*	2019	Lymphoproliferative or myeloid malignancies	22	[^{177}Lu]/[^{90}Y]Pentixather	[168]
Lapa *et al.*	2019	DLBCL	6	[^{177}Lu]/[^{90}Y]Pentixather	[169]
Hänscheid *et al.*	2022	Hematological malignancies	19	[^{177}Lu]/[^{90}Y]Pentixather	[170]
Hartlapp *et al.*	2023	DSRCT	8	[^{90}Y]Pentixather	[90]
Dreher *et al.*	2024	Hematological malignancies	21	[^{90}Y]Pentixather	[171]
Braitsch *et al.*	2025	AML	7	[^{177}Lu]Pentixather	[172]
Dreher *et al.*	2025	MM	38	[^{177}Lu]/[^{90}Y]Pentixather	[8]

MM: multiple myeloma; AML: acute myeloid leukemia; DLBCL: diffuse large B-cell lymphoma; DSRCT: Desmoplastic small round cell tumors.

Ongoing clinical trials are systematically evaluating [^{177}Lu]/[^{90}Y]Pentixather across various malignancies, with particular emphasis on optimal dosing schedules, combination regimens, and patient selection criteria based on comprehensive CXCR4 expression profiling [8,169,171]. As the clinical experience matures, CXCR4-targeted radionuclide therapy is poised to become an important component in the precision oncology arsenal, especially for malignancies characterized by CXCR4 overexpression and dissemination patterns amenable to targeted radionuclide approaches.

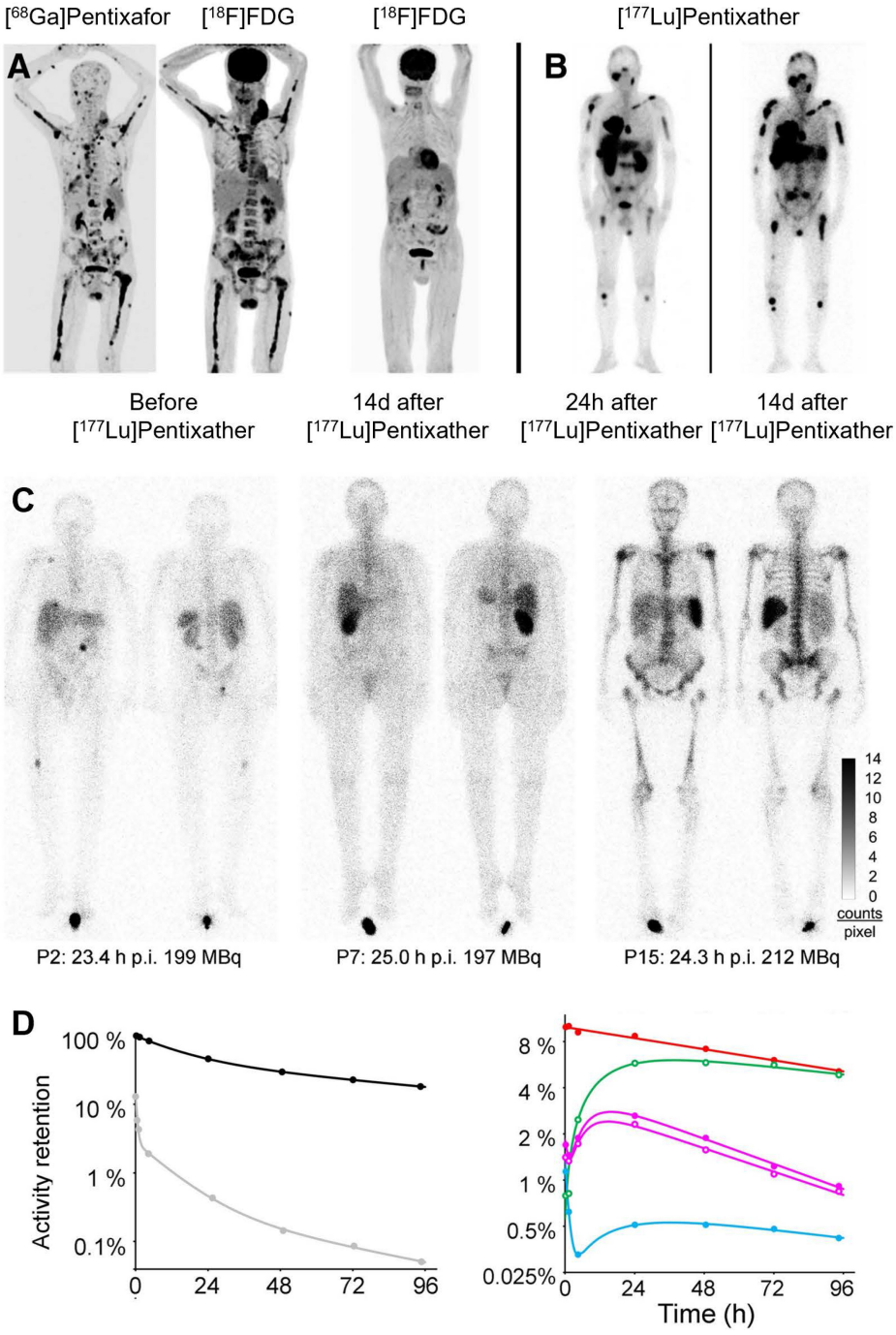

Figure 10. Clinical application of [^{177}Lu]/[^{90}Y]Pentixather. (A) Pre-therapy [^{68}Ga]Pentixafor and [^{18}F]FDG PET/CT MIP in Patient 3 show high CXCR4 expression in multiple FDG-avid extra-/intramedullary myeloma lesions. Post-therapy [^{18}F]FDG PET/CT at 2 weeks after [^{90}Y]Pentixather demonstrates complete metabolic response. **(B)** Scintigraphy in Patient 1 at 24 h and 15 d after 15.2 GBq [^{177}Lu]Pentixather confirms CXCR4 targeting. Altered tumor-to-background ratios reflect decreased background uptake and extended acquisition times at later timepoints. Adapted with permission from [20], copyright © 2016, Society of Nuclear Medicine and Molecular Imaging. **(C)** Variable biodistribution of [^{177}Lu]Pentixather in Patient 2/7 (multiple myeloma) and Patient 15 (pre-B-ALL). While renal uptake reached 5% (single kidney, P7), total renal uptake was only 1.1% in P15. In contrast, P15 showed 3-fold higher bone marrow and 11-fold higher splenic retention. **(D)** Regions of interest for time-activity curves in Patient 3: whole body (black), red marrow (red), liver (green), right/left kidneys (purple solid/open circles), spleen (blue) with fit functions. Gray symbols with fitting curve represent activity retention per liter of whole blood. Adapted with permission from [170], copyright © 2022, Society of Nuclear Medicine and Molecular Imaging.

4.2. Limitations and challenges of CXCR4-targeted radionuclide therapy

While CXCR4-targeted radionuclide therapies, represented by [^{177}Lu]/[^{90}Y]Pentixather, have demonstrated promising initial efficacy in various hematologic malignancies and some solid tumors, it is essential to critically recognize the multiple challenges they face in clinical translation and application [20,33]. The primary challenge stems from the inherent toxicity associated with the target's biological characteristics, rooted in the fundamental contradiction that CXCR4 is not tumor-specific. Its persistent and high expression on normal hematopoietic stem and progenitor cells inevitably leads to significant "off-target" bone marrow toxicity during targeted radionuclide therapy [170]. This results in dose-limiting severe myelosuppression, the direct clinical consequence of which is that the vast majority of existing treatment protocols must incorporate planned autologous hematopoietic stem cell transplantation as a rescue measure [8]. This not only substantially increases the complexity and risks of the treatment but also fundamentally restricts its current applicability to a select minority of patients who are in good physical condition and eligible for transplantation, introducing significant patient selection bias.

Even within tumors exhibiting high CXCR4 expression, significant intra- and inter-tumoral heterogeneity exists in expression levels [175]. Molecular imaging often reveals heterogeneous tracer uptake across different lesions and even within the same lesion. This leads to uneven radiation dose distribution, creating inadequately irradiated "cold spots" that can become sources of tumor recurrence or progression [176–180]. Consequently, the observed therapeutic responses are frequently characterized by limited depth of response and short duration of remission. Furthermore, therapeutic pressure may select for clones with low or negative CXCR4 expression, leading to acquired resistance, which is a key reason for the current lack of clear overall survival benefit data [181]. Compared to the established roles of PSMA and SSTR2 in specific cancer types, the optimal patient population for CXCR4-targeted therapy still requires more precise definition.

5. Conclusion and future perspectives

This comprehensive review has delineated the remarkable progress achieved in targeting the CXCR4/CXCL12 axis for diagnostic and therapeutic purposes in oncology and beyond. The development of the high-affinity CXCR4 ligand Pentixafor and its subsequent radiolabeling with Gallium-68 have established [^{68}Ga]Pentixafor PET as a powerful and versatile non-invasive tool for quantifying CXCR4 expression *in vivo*. Its robust clinical performance has been demonstrated across a remarkably wide spectrum of conditions, spanning hematologic malignancies, solid tumors, endocrine disorders, and inflammatory diseases [16,109–111,114,117,119]. The ability to precisely visualize and quantify CXCR4 expression has proven invaluable for tumor subtyping, staging, prognostic stratification, and treatment response assessment, often outperforming or complementing conventional imaging modalities like [^{18}F]FDG PET/CT, particularly in scenarios involving bone marrow involvement or low metabolic activity [60,64,71,84].

The successful translation of the corresponding therapeutic agent, [^{177}Lu]/[^{90}Y]Pentixather, has completed the radiotheranostic cycle, enabling personalized CXCR4-directed endoradiotherapy [8,172,182,183]. Initial clinical applications, primarily in advanced hematologic malignancies like MM and AML, have confirmed the feasibility and safety of this approach, paving the way for its broader exploration. The paradigm of using [^{68}Ga]Pentixafor for patient selection and treatment planning ensures that therapy is delivered to those most likely to benefit, thereby optimizing the therapeutic index. While the Pentixafor/Pentixather system is the leading clinical CXCR4 theranostic pair, its development benefited from earlier efforts with other agents. Initial trials using radiolabeled AMD3100 confirmed CXCR4 targeting but were limited by poor pharmacokinetics [184]. Other CXCR4-targeting compounds in clinical testing often faced challenges such as low tumor-to-background ratios, high uptake in non-target organs, or stability issues. This highlights that the success of Pentixafor-based agents depends not only on CXCR4 expression but also on their optimized pharmacokinetic and binding properties.

Despite these significant advancements, several challenges and opportunities for future research remain. A primary challenge is the heterogeneity of CXCR4 expression within and between tumors, which can lead to incomplete targeting and potential treatment resistance [185]. Future efforts should focus on elucidating the complex regulation of CXCR4 expression and its dynamic interplay within the tumor microenvironment. Combination therapies represent a particularly promising avenue [186,187]. A positive [^{68}Ga]Pentixafor PET signal reflects the aggregate CXCR4 expression from multiple cellular sources within the lesion, including malignant tumor cells, immune cell infiltration, stromal and progenitor cells in the tumor microenvironment, as well as

non-specific inflammatory processes. Therefore, PET positivity should not be equated solely with tumor cell burden. This biological complexity implies that imaging positivity cannot definitively predict the therapeutic efficacy of [^{177}Lu]/[^{90}Y]Pentixather [172]. If a significant portion of the radiation dose is delivered to non-malignant CXCR4-expressing cells, the therapeutic index may be compromised. Moreover, targeting CXCR4 on stromal or immune cells risks exacerbating on-target toxicity, particularly myelosuppression, without proportionally enhancing tumor cell kill. Consequently, complementary diagnostic methods, such as immunohistochemistry or spatial transcriptomic analysis of biopsy samples, are necessary to deconvolute the cellular origins of CXCR4 expression and better identify patients most likely to benefit from CXCR4-targeted theranostics.

Integrating CXCR4-targeted radionuclide therapy with conventional chemotherapy, immunotherapy, external beam radiotherapy, or other targeted agents could yield synergistic effects by overcoming resistance mechanisms and modulating the immune landscape. For instance, combining CXCR4 inhibition with immune checkpoint blockers could potentially reverse immunosuppression and enhance anti-tumor immunity. The evolution of theranostic agents themselves is another critical frontier [188]. The development of alpha-emitter-labeled Pentixather analogs, such as [^{225}Ac]Pentixather, holds great promise for further improving efficacy, especially against micrometastatic disease, due to the higher linear energy transfer and shorter tissue penetration of alpha particles, which may potentiate greater cytotoxic effects while potentially sparing surrounding healthy tissues. However, when targeting CXCR4, alpha-emitters carry an unacceptable risk of bone marrow toxicity. The high LET radiation renders the bone marrow highly vulnerable, and currently, there is a lack of feasible strategies to overcome this challenge. Consequently, their clinical feasibility remains highly uncertain and requires further validation. Furthermore, the application of artificial intelligence and radiomics to [^{68}Ga]Pentixafor PET imaging data could unlock deeper insights. These approaches may enable the extraction of sub-visual features predictive of treatment response, patient prognosis, and CXCR4 signaling pathway activity, moving towards even more refined precision medicine.

In conclusion, CXCR4-targeted theranostics, exemplified by the [^{68}Ga]Pentixafor /[^{177}Lu]Pentixather pair, has firmly established itself as a transformative strategy in modern medicine. It embodies the core principle of precision medicine, "see what you treat, treat what you see." As ongoing research continues to address current limitations and explore new combinations and technological advancements, CXCR4-directed theranostics is poised to expand its impact, offering renewed hope for patients with a diverse range of CXCR4-driven diseases and solidifying its role as a cornerstone of targeted radionuclide therapy.

Abbreviations

HIV-1: human immunodeficiency virus type 1; MM: multiple myeloma; AML: acute myeloid leukemia; PET: positron emission tomography; SCLC: small cell lung cancer; TBR: tumor-to-background ratio; AMI: acute myocardial infarction; PA: primary aldosteronism; APA: aldosterone-producing adenoma; IHA: idiopathic hyperaldosteronism; NFA: non-functioning adrenal adenomas; CT: computed tomography; SUV: standardized uptake value; ACTH: adrenocorticotropic hormone; MRI: magnetic resonance imaging; MZL: marginal zone lymphoma; WM/LPL: waldenström macroglobulinemia/ lymphoplasmacytic lymphoma; MCL: mantle cell lymphoma; CNSL: central nervous system lymphoma; CLL: chronic lymphocytic leukemia; MALT: mucosa-associated lymphoid tissue; GBM: glioblastoma; R-CT: radiochemotherapy; HNSCC: head and neck squamous cell carcinoma; NPC: nasopharyngeal carcinoma; NSCLC: non-small cell lung cancer; ACC: adrenal cortical carcinoma.

Acknowledgements

AI tool (DeepSeek) was used for language assistance during writing, but not for content generation. This study was supported by Innovative Drug Research and Development-National Science and Technology Major Project (2025ZD1803400), National Natural Science Foundation of China (82202233) and Construction Project of Shanghai Key Laboratory of Molecular Imaging (KFKT-2025-09).

Author contributions

Conceptualizing structure: Biao Yang, Mengting Li and Xiaoli Lan; Preparing figures and/or tables: Biao Yang and Wenzhu Hu; Writing—original draft: Biao Yang; Writing—review and editing: Mengting Li and Xiaoli Lan; Supervision: Mengting Li, Xiaoli Lan, Xiao Zhang, Yongkang Gai, Rui An and Chunxia Qin. All authors reviewed the article and approved the final version of the manuscript.

Competing interests

The authors have declared that no competing interest exists.

References

1. Teicher BA, Fricker SP. CXCL12 (SDF-1)/CXCR4 pathway in cancer. Clin Cancer Res. 2010; 16: 2927-31.
2. Duda DG, Kozin SV, Kirkpatrick ND, Xu L, Fukumura D, Jain RK. CXCL12 (SDF1alpha)-CXCR4/CXCR7 pathway inhibition: an emerging sensitizer for anticancer therapies? Clin Cancer Res. 2011; 17: 2074-80.
3. Heidegger I, Fotakis G, Offermann A, Goveia J, Daum S, Salcher S, *et al.* Comprehensive characterization of the prostate tumor microenvironment identifies CXCR4/CXCL12 crosstalk as a novel antiangiogenic therapeutic target in prostate cancer. Mol Cancer. 2022; 21: 132.
4. Cao C, Xu M, Peng T, Liu X, Lin S, Xu Y, *et al.* Blocking CXCR4+ CD4+ T cells reprograms Treg-mediated immunosuppression via modulating the Rho-GTPase/NF-κB signaling axis. Genome Med. 2025; 17: 85.
5. Marichannegowda MH, Setua S, Bose M, Sanders-Buell E, King D, Zemil M, *et al.* Transmission of highly virulent CXCR4 tropic HIV-1 through the mucosal route in an individual with a wild-type CCR5 genotype. EBioMedicine. 2024; 109: 105410.
6. Zhang Z, Zhang H, Zheng L, Chen S, Du S, Xiao J, *et al.* CXCR4 mediated recognition of HIV envelope spike and inhibition by CXCL12. Nat Commun. 2025; 16: 8653.
7. Demmer O, Dijkgraaf I, Schumacher U, Marinelli L, Cosconati S, Gourni E, *et al.* Design, synthesis, and functionalization of dimeric peptides targeting chemokine receptor CXCR4. J Med Chem. 2011; 54: 7648-62.
8. Dreher N, Dörrler AL, Kraus S, Rasche L, Higuchi T, Samnick S, *et al.* Myeloablative Radioligand Therapy Targeting C-X-C Motif Chemokine Receptor 4 in Advanced Multiple Myeloma. Clin Nucl Med. 2025; 50: 495-500.
9. Wang X, Wang X, Su J, Wang D, Feng W, Wang X, *et al.* A Dual-Function LipoAraN-E5 Coloaded with N4-Myristyloxycarbonyl-1-β-d-arabinofuranosylcytosine (AraN) and a CXCR4 Antagonistic Peptide (E5) for Blocking the Dissemination of Acute Myeloid Leukemia. ACS Nano. 2024; 18: 27917-32.
10. Wang K, Wang C, Yang H, Chen G, Wang K, Ji P, *et al.* A dual-targeting peptide-drug conjugate based on CXCR4 and FOLR1 inhibits triple-negative breast cancer. Acta Pharm Sin B. 2025; 15: 4995-5009.
11. Cordier C, Haustrate A, Mihalache A, Duval E, Desruelles E, Spriet C, *et al.* Targeting TRPV6/CXCR4 complexes prevents castration-resistant prostate cancer metastasis to the bone. Signal Transduct Target Ther. 2025; 10: 287.
12. Tao M, Liu W, Chen J, Liu R, Zou J, Yu B, *et al.* Transcriptome Landscape of Cancer-Associated Fibroblasts in Human PDAC. Adv Sci (Weinh). 2025; 12: e2415196.
13. Ullah TR. The role of CXCR4 in multiple myeloma: Cells' journey from bone marrow to beyond. J Bone Oncol. 2019; 17: 100253.
14. Soe Y, Kawai H, Eain HS, Yoshida S, Oo MW, Min ZZ, *et al.* CXCR4 Inhibition Induces Tumor Necrosis by Selectively Targeting the Proliferating Blood Vessels in Oral Squamous Cell Carcinoma. J Cancer. 2025; 16: 4055-70.
15. Abbasifard M, Mohammadi-Shahrokhi V, Khorramdelazad H. Stromal-derived factor-1: The glycoprotein fueling autoimmune storms via CXCR4 and CXCR7. Int J Biol Macromol. 2025; 321: 146374.
16. Diekmann J, König T, Hess A, Zwadlo C, Schäfer A, Ross TL, *et al.* CXCR4 PET/CT Predicts Left Ventricular Recovery 8 Months After Acute Myocardial Infarction. J Nucl Med. 2025; 66: 1750-6.
17. Chen Y, Yuan H, Tan X, Shang Y, Sun X, Wang P, *et al.* CXCR4-Targeted 68Ga-Pentixafor PET/CT Imaging in Inflammatory Bowel Disease. Clin Nucl Med. 2024; 49: 817-21.
18. Rueda A, Serna N, Mangues R, Villaverde A, Unzueta U. Targeting the chemokine receptor CXCR4 for cancer therapies. Biomark Res. 2025; 13: 68.
19. Wester HJ, Keller U, Schottelius M, Beer A, Philipp-Abbrederis K, Hoffmann F, *et al.* Disclosing the CXCR4 expression in lymphoproliferative diseases by targeted molecular imaging. Theranostics. 2015; 5: 618-30.
20. Herrmann K, Schottelius M, Lapa C, Osl T, Poschenrieder A, Hänscheid H, *et al.* First-in-Human Experience of CXCR4-Directed Endoradiotherapy with 177Lu- and 90Y-Labeled Pentixather in Advanced-Stage Multiple Myeloma with Extensive Intra- and Extramedullary Disease. J Nucl Med. 2016; 57: 248-51.
21. Trotta AM, Aurilio M, D'Alterio C, Ieranò C, Di Martino D, Barbieri A, *et al.* Novel Peptide-Based PET Probe for Non-invasive Imaging of C-X-C Chemokine Receptor Type 4 (CXCR4) in Tumors. J Med Chem. 2021; 64: 3449-61.
22. Gaonkar RH, Schmidt YT, Mansi R, Almeida-Hernandez Y, Sanchez-Garcia E, Harms M, *et al.* Development of a New Class of CXCR4-Targeting Radioligands Based on the Endogenous Antagonist EPI-X4 for Oncological Applications. J Med Chem. 2023; 66: 8484-97.
23. Cheng K, Wang S, Liu T, Pei J, Wang S, Liu J, *et al.* PET imaging of CXCR4 expression using [18F]AlF-NOTA-QHY-04 for hematologic malignancy and solid tumors. Theranostics. 2024; 14: 6337-49.
24. Pei J, Cheng K, Liu T, Gao M, Wang S, Xu S, *et al.* Early, non-invasive detection of radiation-induced lung injury using PET/CT by targeting CXCR4. Eur J Nucl Med Mol Imaging. 2024; 51: 1109-20.
25. Gourni E, Demmer O, Schottelius M, D'Alessandria C, Schulz S, Dijkgraaf I, *et al.* PET of CXCR4 expression by a (68)Ga-labeled highly specific targeted contrast agent. J Nucl Med. 2011; 52: 1803-10.
26. Hennrich U, Seyler L, Schäfer M, Bauder-Wüst U, Eisenhut M, Semmler W, *et al.* Synthesis and in vitro evaluation of 68Ga-DOTA-4-FBn-TN14003, a novel tracer for the imaging of CXCR4 expression. Bioorg Med Chem. 2012; 20: 1502-10.
27. George GPC, Stevens E, Åberg O, Nguyen QD, Pisaneschi F, Spivey AC, *et al.* Preclinical evaluation of a CXCR4-specific (68)Ga-labelled TN14003 derivative for cancer PET imaging. Bioorg Med Chem. 2014; 22: 796-803.
28. Poty S, Gourni E, Désogère P, Boschetti F, Goze C, Maecke HR, *et al.* AMD3100: A Versatile Platform for CXCR4 Targeting (68)Ga-Based Radiopharmaceuticals. Bioconjug Chem. 2016; 27: 752-61.
29. Poschenrieder A, Schottelius M, Schwaiger M, Wester HJ. Preclinical evaluation of [(68)Ga]NOTA-pentixafor for PET imaging of CXCR4 expression in vivo-a comparison to [(68)Ga]pentixafor. EJNMMI Res. 2016; 6: 70.
30. Hyafil F, Pelisek J, Laitinen I, Schottelius M, Mohring M, Döring Y, *et al.* Imaging the Cytokine Receptor CXCR4 in Atherosclerotic Plaques with the Radiotracer 68Ga-Pentixafor for PET. J Nucl Med. 2017; 58: 499-506.
31. Herrmann K, Lapa C, Wester HJ, Schottelius M, Schiepers C, Eberlein U, *et al.* Biodistribution and radiation dosimetry for the chemokine receptor CXCR4-targeting probe 68Ga-pentixafor. J Nucl Med. 2015; 56: 410-6.
32. Philipp-Abbrederis K, Herrmann K, Knop S, Schottelius M, Eiber M, Lückerath K, *et al.* In vivo molecular imaging of chemokine receptor CXCR4 expression in patients with advanced multiple myeloma. EMBO Mol Med. 2015; 7: 477-87.
33. Habringer S, Lapa C, Herhaus P, Schottelius M, Istvanffy R, Steiger K, *et al.* Dual Targeting of Acute Leukemia and Supporting Niche by CXCR4-Directed Theranostics. Theranostics. 2018; 8: 369-83.
34. Benčurová K, Friske J, Anderla M, Mayrhofer M, Wanek T, Nics L, *et al.* CAM-Xenograft Model Provides Preclinical Evidence for the Applicability of [68Ga]Ga-Pentixafor in CRC Imaging. Cancers (Basel). 2022; 14: 5549.
35. Glasenapp A, Derlin K, Gutberlet M, Hess A, Ross TL, Wester HJ, *et al.* Molecular Imaging of Inflammation and Fibrosis in Pressure Overload Heart Failure. Circ Res. 2021; 129: 369-82.
36. Wang Z, Zhang M, Wang L, Wang S, Kang F, Li G, *et al.* Prospective Study of (68)Ga-NOTA-NFB: Radiation Dosimetry in Healthy Volunteers and First Application in Glioma Patients. Theranostics. 2015; 5: 882-9.
37. Reiter T, Kircher M, Schirbel A, Werner RA, Kropf S, Ertl G, *et al.* Imaging of C-X-C Motif Chemokine Receptor CXCR4 Expression After Myocardial Infarction With [68Ga]Pentixafor-PET/CT in Correlation With Cardiac MRI. JACC Cardiovasc Imaging. 2018; 11: 1541-3.
38. Vag T, Gerngross C, Herhaus P, Eiber M, Philipp-Abbrederis K, Graner FP, *et al.* First Experience with Chemokine Receptor CXCR4-Targeted PET Imaging of Patients with Solid Cancers. J Nucl Med. 2016; 57: 741-6.
39. Lapa C, Lückerath K, Rudelius M, Schmid JS, Schoene A, Schirbel A, *et al.* [68Ga]Pentixafor-PET/CT for imaging of chemokine receptor 4 expression in small cell lung cancer--initial experience. Oncotarget. 2016; 7: 9288-95.
40. Lapa C, Lückerath K, Kleinlein I, Monoranu CM, Linsenmann T, Kessler AF, *et al.* (68)Ga-Pentixafor-PET/CT for Imaging of Chemokine Receptor 4 Expression in Glioblastoma. Theranostics. 2016; 6: 428-34.
41. Herhaus P, Habringer S, Philipp-Abbrederis K, Vag T, Gerngross C, Schottelius M, *et al.* Targeted positron emission tomography imaging of CXCR4 expression in patients with acute myeloid leukemia. Haematologica. 2016; 101: 932-40.
42. Bluemel C, Hahner S, Heinze B, Fassnacht M, Kroiss M, Bley TA, *et al.* Investigating the Chemokine Receptor 4 as Potential Theranostic Target in Adrenocortical Cancer Patients. Clin Nucl Med. 2017; 42: e29-34.
43. Lapa C, Schreder M, Schirbel A, Samnick S, Kortüm KM, Herrmann K, *et al.* [68Ga]Pentixafor-PET/CT for imaging of chemokine receptor CXCR4 expression in multiple myeloma - Comparison to [18F]FDG and laboratory values. Theranostics. 2017; 7: 205-12.
44. Derlin T, Gueler F, Bräsen JH, Schmitz J, Hartung D, Herrmann TR, *et al.* Integrating MRI and Chemokine Receptor CXCR4-Targeted PET for Detection of Leukocyte Infiltration in Complicated Urinary Tract Infections After Kidney Transplantation. J Nucl Med. 2017; 58: 1831-7.
45. Werner RA, Weich A, Higuchi T, Schmid JS, Schirbel A, Lassmann M, *et al.* Imaging of Chemokine Receptor 4 Expression in Neuroendocrine Tumors - a Triple Tracer Comparative Approach. Theranostics. 2017; 7: 1489-98.
46. Herhaus P, Habringer S, Vag T, Steiger K, Slotta-Huspenina J, Gerngroß C, *et al.* Response assessment with the CXCR4-directed positron emission tomography tracer [68Ga]Pentixafor in a patient with extranodal marginal zone lymphoma of the orbital cavities. EJNMMI Res. 2017; 7: 51.
47. Lapa C, Kircher S, Schirbel A, Rosenwald A, Kropf S, Pelzer T, *et al.* Targeting CXCR4 with [68Ga]Pentixafor: a suitable theranostic approach in pleural mesothelioma? Oncotarget. 2017; 8: 96732-7.
48. Bouter C, Meller B, Sahlmann CO, Staab W, Wester HJ, Kropf S, *et al.* 68Ga-Pentixafor PET/CT Imaging of Chemokine Receptor CXCR4 in Chronic Infection of the Bone: First Insights. J Nucl Med. 2018; 59: 320-6.
49. Weiberg D, Thackeray JT, Daum G, Sohns JM, Kropf S, Wester HJ, *et al.* Clinical Molecular Imaging of Chemokine Receptor CXCR4 Expression in Atherosclerotic Plaque Using 68Ga-Pentixafor PET: Correlation with Cardiovascular Risk Factors and Calcified Plaque Burden. J Nucl Med. 2018; 59: 266-72.
50. Li X, Heber D, Leike T, Beitzke D, Lu X, Zhang X, *et al.* [68Ga]Pentixafor-PET/MRI for the detection of Chemokine receptor 4 expression in atherosclerotic plaques. Eur J Nucl Med Mol Imaging. 2018; 45: 558-66.

51. Mayerhoefer ME, Jaeger U, Staber P, Raderer M, Wadsak W, Pfaff S, *et al.* [68Ga]Ga-Pentixafor PET/MRI for CXCR4 Imaging of Chronic Lymphocytic Leukemia: Preliminary Results. Invest Radiol. 2018; 53: 403-8.
52. Derlin T, Sedding DG, Dutzmann J, Haghikia A, König T, Napp LC, *et al.* Imaging of chemokine receptor CXCR4 expression in culprit and nonculprit coronary atherosclerotic plaque using motion-corrected [68Ga]pentixafor PET/CT. Eur J Nucl Med Mol Imaging. 2018; 45: 1934-44.
53. Bouter Y, Meller B, Sahlmann CO, Wolf BJ, Langer L, Bankstahl JP, *et al.* Immunohistochemical detection of chemokine receptor 4 expression in chronic osteomyelitis confirms specific uptake in 68Ga-Pentixafor-PET/CT. Nuklearmedizin. 2018; 57: 198-203.
54. Li X, Yu W, Wollenweber T, Lu X, Wei Y, Beitzke D, *et al.* [68Ga]Pentixafor PET/MR imaging of chemokine receptor 4 expression in the human carotid artery. Eur J Nucl Med Mol Imaging. 2019; 46: 1616-25.
55. Luo Y, Cao X, Pan Q, Li J, Feng J, Li F. 68Ga-Pentixafor PET/CT for Imaging of Chemokine Receptor 4 Expression in Waldenström Macroglobulinemia/Lymphoplasmacytic Lymphoma: Comparison to 18F-FDG PET/CT. J Nucl Med. 2019; 60: 1724-9.
56. Breun M, Monoranu CM, Kessler AF, Matthies C, Löhr M, Hagemann C, *et al.* [68Ga]-Pentixafor PET/CT for CXCR4-Mediated Imaging of Vestibular Schwannomas. Front Oncol. 2019; 9: 503.
57. Haug AR, Leisser A, Wadsak W, Mitterhauser M, Pfaff S, Kropf S, *et al.* Prospective non-invasive evaluation of CXCR4 expression for the diagnosis of MALT lymphoma using [68Ga]Ga-Pentixafor-PET/MRI. Theranostics. 2019; 9: 3653-8.
58. Werner RA, Kircher S, Higuchi T, Kircher M, Schirbel A, Wester HJ, *et al.* CXCR4-Directed Imaging in Solid Tumors. Front Oncol. 2019; 9: 770.
59. Kircher M, Tran-Gia J, Kemmer L, Zhang X, Schirbel A, Werner RA, *et al.* Imaging Inflammation in Atherosclerosis with CXCR4-Directed 68Ga-Pentixafor PET/CT: Correlation with 18F-FDG PET/CT. J Nucl Med. 2020; 61: 751-6.
60. Pan Q, Cao X, Luo Y, Li J, Feng J, Li F. Chemokine receptor-4 targeted PET/CT with 68Ga-Pentixafor in assessment of newly diagnosed multiple myeloma: comparison to 18F-FDG PET/CT. Eur J Nucl Med Mol Imaging. 2020; 47: 537-46.
61. Ding J, Zhang Y, Wen J, Zhang H, Wang H, Luo Y, *et al.* Imaging CXCR4 expression in patients with suspected primary hyperaldosteronism. Eur J Nucl Med Mol Imaging. 2020; 47: 2656-65.
62. Herhaus P, Lipkova J, Lammer F, Yakushev I, Vag T, Slotta-Huspenina J, *et al.* CXCR4-Targeted PET Imaging of Central Nervous System B-Cell Lymphoma. J Nucl Med. 2020; 61: 1765-71.
63. Pan Q, Luo Y, Zhang Y, Chang L, Li J, Cao X, *et al.* Preliminary evidence of imaging of chemokine receptor-4-targeted PET/CT with [68Ga]pentixafor in non-Hodgkin lymphoma: comparison to [18F]FDG. EJNMMI Res. 2020; 10: 89.
64. Lawal IO, Popoola GO, Mahapane J, Kaufmann J, Davis C, Ndlovu H, *et al.* [68Ga]Ga-Pentixafor for PET Imaging of Vascular Expression of CXCR-4 as a Marker of Arterial Inflammation in HIV-Infected Patients: A Comparison with 18F[FDG] PET Imaging. Biomolecules. 2020; 10: 1629.
65. Starzer AM, Berghoff AS, Traub-Weidinger T, Haug AR, Widhalm G, Hacker M, *et al.* Assessment of Central Nervous System Lymphoma Based on CXCR4 Expression In Vivo Using 68Ga-Pentixafor PET/MRI. Clin Nucl Med. 2021; 46: 16-20.
66. Mayerhoefer ME, Raderer M, Lamm W, Pichler V, Pfaff S, Weber M, *et al.* CXCR4 PET imaging of mantle cell lymphoma using [68Ga]Pentixafor: comparison with [18F]FDG-PET. Theranostics. 2021; 11: 567-78.
67. Linde P, Baues C, Wegen S, Trommer M, Quaas A, Rosenbrock J, *et al.* Pentixafor PET/CT for imaging of chemokine receptor 4 expression in esophageal cancer - a first clinical approach. Cancer Imaging. 2021; 21: 22.
68. Duell J, Krummenast F, Schirbel A, Klassen P, Samnick S, Rauert-Wunderlich H, *et al.* Improved Primary Staging of Marginal-Zone Lymphoma by Addition of CXCR4-Directed PET/CT. J Nucl Med. 2021; 62: 1415-21.
69. Weich A, Werner RA, Buck AK, Hartrampf PE, Serfling SE, Scheurlen M, *et al.* CXCR4-Directed PET/CT in Patients with Newly Diagnosed Neuroendocrine Carcinomas. Diagnostics (Basel). 2021; 11: 605.
70. Werner RA, Hess A, Koenig T, Diekmann J, Derlin T, Melk A, *et al.* Molecular imaging of inflammation crosstalk along the cardio-renal axis following acute myocardial infarction. Theranostics. 2021; 11: 7984-94.
71. Pan Q, Cao X, Luo Y, Li J, Li F. Semi-quantitative measurements of chemokine receptor 4-targeted 68Ga-pentixafor PET/CT in response assessment of Waldenström macroglobulinemia/lymphoplasmacytic lymphoma. EJNMMI Res. 2021; 11: 110.
72. Kuyumcu S, Isik EG, Tiryaki TO, Has-Simsek D, Sanli Y, Buyukkaya F, *et al.* Prognostic significance of 68Ga-Pentixafor PET/CT in multiple myeloma recurrence: a comparison to 18F-FDG PET/CT and laboratory results. Ann Nucl Med. 2021; 35: 1147-56.
73. Lewis R, Habringer S, Kircher M, Hefter M, Peuker CA, Werner R, *et al.* Investigation of spleen CXCR4 expression by [68Ga]Pentixafor PET in a cohort of 145 solid cancer patients. EJNMMI Res. 2021; 11: 77.
74. Jacobs SM, Wesseling P, de Keizer B, Tolboom N, Ververs FFT, Krijger GC, *et al.* CXCR4 expression in glioblastoma tissue and the potential for PET imaging and treatment with [68Ga]Ga-Pentixafor /[177Lu]Lu-Pentixather. Eur J Nucl Med Mol Imaging. 2022; 49: 481-91.
75. Kraus S, Dierks A, Rasche L, Kertels O, Kircher M, Schirbel A, *et al.* 68Ga-Pentixafor PET/CT for Detection of Chemokine Receptor CXCR4 Expression in Myeloproliferative Neoplasms. J Nucl Med. 2022; 63: 96-9.
76. Mayerhoefer ME, Raderer M, Lamm W, Weber M, Kiesewetter B, Rohrbeck J, *et al.* CXCR4 PET/MRI for follow-up of gastric mucosa-associated lymphoid tissue lymphoma after first-line Helicobacter pylori eradication. Blood. 2022; 139: 240-4.
77. Chen Z, Yang A, Zhang J, Chen A, Zhang Y, Huang C, *et al.* CXCR4-Directed PET/CT with [68Ga]Pentixafor in Central Nervous System Lymphoma: A Comparison with [18F]FDG PET/CT. Mol Imaging Biol. 2022; 24: 416-24.
78. Kwon D, Takata K, Zhang Z, Chong L, Fraser B, Zeisler J, *et al.* Targeting Refractory Mantle Cell Lymphoma for Imaging and Therapy Using C-X-C Chemokine Receptor Type 4 Radioligands. Clin Cancer Res. 2022; 28: 1628-39.
79. Buck AK, Haug A, Dreher N, Lambertini A, Higuchi T, Lapa C, *et al.* Imaging of C-X-C Motif Chemokine Receptor 4 Expression in 690 Patients with Solid or Hematologic Neoplasms Using 68Ga-Pentixafor PET. J Nucl Med. 2022; 63: 1687-92.
80. Serfling SE, Lapa C, Dreher N, Hartrampf PE, Rowe SP, Higuchi T, *et al.* Impact of Tumor Burden on Normal Organ Distribution in Patients Imaged with CXCR4-Targeted [68Ga]Ga-PentixaFor PET/CT. Mol Imaging Biol. 2022; 24: 659-65.
81. Ding J, Tong A, Hacker M, Feng M, Huo L, Li X. Usefulness of 68Ga-Pentixafor PET/CT on Diagnosis and Management of Cushing Syndrome. Clin Nucl Med. 2022; 47: 669-76.
82. Watts A, Singh B, Singh H, Kaur H, Bal A, Vohra M, *et al.* 68Ga-Pentixafor PET/CT Demonstrating In Vivo CXCR4 Receptor Overexpression in Rare Lung Malignancies: Correlation with Histologic and Histochemical Findings. J Nucl Med Technol. 2022; 50: 278-81.
83. Shekhawat AS, Singh B, Malhotra P, Watts A, Basher R, Kaur H, *et al.* Imaging CXCR4 receptors expression for staging multiple myeloma by using 68Ga-Pentixafor PET/CT: comparison with 18F-FDG PET/CT. Br J Radiol. 2022; 95: 20211272.
84. Lu X, Calabretta R, Wadsak W, Haug AR, Mayerhöfer M, Raderer M, *et al.* Imaging Inflammation in Atherosclerosis with CXCR4-Directed [68Ga]PentixaFor PET/MRI-Compared with [18F]FDG PET/MRI. Life (Basel). 2022; 12: 1039.
85. Kraus S, Klassen P, Kircher M, Dierks A, Habringer S, Gäble A, *et al.* Reduced splenic uptake on 68Ga-Pentixafor-PET/CT imaging in multiple myeloma - a potential imaging biomarker for disease prognosis. Theranostics. 2022; 12: 5986-94.
86. Gao Y, Ding J, Cui Y, Li T, Sun H, Zhao D, *et al.* Functional nodules in primary aldosteronism: identification of CXCR4 expression with 68Ga-pentixafor PET/CT. Eur Radiol. 2023; 33: 996-1003.
87. Watts A, Singh B, Singh H, Bal A, Kaur H, Dhanota N, *et al.* [68Ga]Ga-Pentixafor PET/CT imaging for in vivo CXCR4 receptor mapping in different lung cancer histologic sub-types: correlation with quantitative receptors' density by immunochemistry techniques. Eur J Nucl Med Mol Imaging. 2023; 50: 1216-27.
88. Mayerhoefer ME, Raderer M, Weber M, Lamm W, Kiesewetter B, Hacker M, *et al.* 68Ga-Pentixafor PET/MRI for Treatment Response Assessment in Mantle Cell Lymphoma: Comparison Between Changes in Lesion CXCR4 Expression on PET and Lesion Size and Diffusivity on MRI. Clin Nucl Med. 2023; 48: 557-62.
89. Kosmala A, Seifert S, Schneid S, Dreher N, Higuchi T, Weich A, *et al.* Lymphoma-Sink Effect in Marginal Zone Lymphoma Based on CXCR4-Targeted Molecular Imaging. Mol Imaging Biol. 2023; 25: 758-64.
90. Hartlapp I, Hartrampf PE, Serfling SE, Wild V, Weich A, Rasche L, *et al.* CXCR4-Directed Imaging and Endoradiotherapy in Desmoplastic Small Round Cell Tumors. J Nucl Med. 2023; 64: 1424-30.
91. Roustaei H, Norouzbeigi N, Vosoughi H, Aryana K. A dataset of [68Ga]Ga-Pentixafor PET/CT images of patients with high-grade Glioma. Data Brief. 2023; 48: 109236.
92. Zheng Y, Long T, Peng N, Zhen M, Ye Q, Zhang Z, *et al.* The Value of Targeting CXCR4 With 68Ga-Pentixafor PET/CT for Subtyping Primary Aldosteronism. J Clin Endocrinol Metab. 2023; 109: 171-82.
93. Zhi Y, Werner RA, Schirbel A, Higuchi T, Buck AK, Kosmala A, *et al.* Diagnostic efficacy of C-X-C motif chemokine receptor 4-directed PET/CT in newly diagnosed head and neck squamous cell carcinoma - a head-to-head comparison with [18F]FDG. Am J Nucl Med Mol Imaging. 2023; 13: 208-16.
94. Kosmala A, Duell J, Schneid S, Serfling SE, Higuchi T, Weich A, *et al.* Chemokine receptor-targeted PET/CT provides superior diagnostic performance in newly diagnosed marginal zone lymphoma patients: a head-to-head comparison with [18F]FDG. Eur J Nucl Med Mol Imaging. 2024; 51: 749-55.
95. Dreher N, Hahner S, Fuß CT, Schlötelburg W, Hartrampf PE, Serfling SE, *et al.* CXCR4-directed PET/CT with [68Ga]Ga-pentixafor in solid tumors-a comprehensive analysis of imaging findings and comparison with histopathology. Eur J Nucl Med Mol Imaging. 2024; 51: 1383-94.
96. Jena SR, Watts A, Aggarwal P, Bachhal V, Kaur H, Dhingra K, *et al.* 68Ga-Pentixafor PET/CT for in-vivo mapping of CXCR4 receptors as potential radiotheranostic targets in soft tissue and bone sarcoma: preliminary results. Nucl Med Commun. 2024; 45: 229-35.
97. Waheed A, Singh B, Watts A, Kaur H, Singh H, Dhingra K, *et al.* 68Ga-Pentixafor PET/CT for In Vivo Imaging of CXCR4 Receptors in Glioma Demonstrating a Potential for Response Assessment to Radiochemotherapy: Preliminary Results. Clin Nucl Med. 2024; 49: e141-8.
98. Yin X, Ai K, Luo J, Liu W, Ma X, Zhou L, *et al.* A comparison of the performance of 68Ga-Pentixafor PET/CT versus adrenal vein sampling for

subtype diagnosis in primary aldosteronism. Front Endocrinol (Lausanne). 2024; 15: 1291775.
99. Liu M, Chen X, Ding H, Shu Q, Zheng Y, Chen Y, *et al*. Comparison of [18F]FDG and [68Ga]pentixafor PET/CT in Nasopharyngeal Carcinoma. Mol Imaging Biol. 2024; 26: 658-67.
100. Pan Q, Cao X, Li J, Li F, Luo Y. Different extramedullary disease shown in chemokine receptor 4 targeted PET/CT with [68Ga]Ga-pentixafor in patients with Waldenström macroglobulinemia and smoldering disease. Nucl Med Commun. 2024; 45: 727-35.
101. Schloetelburg W, Hartrampf PE, Kosmala A, Serfling SE, Dreher N, Schirbel A, *et al*. Predictive value of C-X-C motif chemokine receptor 4-directed molecular imaging in patients with advanced adrenocortical carcinoma. Eur J Nucl Med Mol Imaging. 2024; 51: 3643-50.
102. Hadebe B, Harry L, Gabela L, Masikane S, Patel M, Zwane S, *et al*. Chemokine Receptor-4 Targeted PET/CT Imaging with 68Ga-Pentixafor in Head and Neck Cancer-A Comparison with 18F-FDG and CXCR4 Immunohistochemistry. Diagnostics (Basel). 2024; 14: 1375.
103. Roustaei H, Vosoughi H, Askari E, Aziz Kalantari B, Norouzbeigi N, Anvari K, *et al*. [68 Ga]Ga-CXCR4 PET/CT imaging in high-grade glioma for assessment of CXCR4 receptor expression. Eur J Radiol. 2024; 180: 111694.
104. Kopp CR, Sharma SK, Krishnaraju VS, Sood A, Kumar R, Sinha A, *et al*. Chemokine receptor CXCR4 based positron emission tomography imaging in systemic sclerosis-related interstitial lung disease. Rheumatology (Oxford). 2024; keae503.
105. Wu Y, Wu Y, Yao B, Ren S, Wu S, Rui W, *et al*. Diagnostic Accuracy and Value of CXCR4-targeted PET/MRI Using 68Ga-Pentixafor for Tumor Localization in Cushing Disease. Radiology. 2024; 313: e233469.
106. Yang Q, Zhang F, Hao Z, Zhuang J, Huo L. Chemokine Receptor 4-Targeted PET/CT with [68Ga]pentixather in Newly Diagnosed Multiple Myeloma: a Comparative Study with [68Ga]pentixafor PET/CT. Mol Imaging Biol. 2024; 26: 986-94.
107. Zuo R, Liu S, Ren X, Li W, Xia Z, Xu L, *et al*. Typing diagnostic value of 68Ga-pentixafor PET/CT for patients with primary aldosteronism and unilateral nodules. Endocrine. 2025; 87: 314-24.
108. Yi T, Lu D, Cui Y, Zhang Z, Yang X, Zhang J, *et al*. 68Ga-pentixafor PET/CT Is a Supplementary Method for Primary Aldosteronism Subtyping Compared with Adrenal Vein Sampling. Mol Imaging Biol. 2025; 27: 142-50.
109. Zhang X, Song Y, Jing Y, Hu J, Shen H, Zhang A, *et al*. Comparison of Different Diagnostic Criteria of 68Ga-Pentixafor PET/CT for the Classification of Primary Aldosteronism. J Clin Endocrinol Metab. 2025; 110: e2583-90.
110. Chen Z, Liu H, Yang A, Liao J, Wu Z, Chen J, *et al*. 68Ga-Pentixafor PET in Combination With MRI Improves the Differential Diagnosis of Glioblastoma and Primary Central Nervous System Lymphoma. Clin Nucl Med. 2025; 50: 324-31.
111. Kosmala A, Hasenauer N, Serfling SE, Michalski K, Fröhlich M, Dreher N, *et al*. C-X-C motif chemokine receptor 4-directed PET signal in the arterial tree is not consistently linked to calcified plaque burden and cardiovascular risk. Theranostics. 2025; 15: 804-14.
112. Li M, Guan L, Yang L, Li W, Xia Z, Mao M, *et al*. 68Ga-Pentixafor PET/CT for the assessment of therapeutic outcomes following superselective adrenal arterial embolization in patients with primary aldosteronism. EJNMMI Res. 2025; 15: 5.
113. Zheng G, Ding J, Gao Y, Liu S, Yan X, Wang W, *et al*. 68Ga-pentixafor PET/CT in guiding surgical management of primary aldosteronism. J Clin Transl Endocrinol. 2025; 39: 100384.
114. Wang R, Gao X, Peng X, Wang J, Xiang J, Li L, *et al*. Clinical Application of 68Ga-Pentixafor PET/CT for the Detection of Thymoma: A Pilot Study. Clin Nucl Med. 2025; 50: 388-93.
115. Kaur H, Kumar S, Watts A, Singh C, Sachdeva MUS, Sreedharanunni S, *et al*. 68Ga-Pentixafor PET/CT-Based Response Evaluation and its Prognostic Value in Multiple Myeloma: Comparison With IMWG and 18F-FDG-Based Response. Clin Nucl Med. 2025; 50: e331-9.
116. Gauthaman DK, Muthukrishnan I, Acharya KA, Simon S. Ga-68 Pentixafor PET/CT in multiple myeloma and its correlation with clinical parameters: institutional pilot study. Ann Nucl Med. 2025; 39: 588-99.
117. Hadebe B, Harry L, Gabela L, Nxasana T, Ndlovu N, Pillay V, *et al*. Comparing 68Ga-Pentixafor,18F-FDG PET/CT and Chemokine Receptor 4 Immunohistochemistry Staining in Breast Cancer: A Prospective Cross Sectional Study. Cancers (Basel). 2025; 17: 763.
118. Zheng WC, Chen SM, Qiu QR, Li XD, Lin F, Shen XM, *et al*. Total or partial adrenalectomy for aldosterone-producing adenoma: can 68Ga-Pentixafor PET/CT predict surgical outcomes? Eur J Nucl Med Mol Imaging. 2025; 52: 3632-42.
119. Meng X, Quan Z, Fan L, Zhang M, Li G, Xu M, *et al*. Added value of multiparametric MRI for diagnosing subcentimeter functional adrenal nodules in primary aldosteronism using CXCR4-targeted PET/MRI. Eur J Nucl Med Mol Imaging. 2025; 52: 5189-99.
120. Pan Q, Chen Z, Liu S, Zhang H, Feng J, Miao W, *et al*. Reduced splenic uptake of [68Ga]Ga-Pentixafor following first-line chemotherapy is associated with poor prognosis in patients with newly diagnosed multiple myeloma. EJNMMI Res. 2025; 15: 74.
121. Zhoufei F, Qixiang Z, Wei Z, Jinxiu L, Feng P, Han C. The utility of 68Ga-pentixafor PET/CT in superselective adrenal artery embolization(SAAE) for treating aldosterone adenomas. Eur J Nucl Med Mol Imaging. 2026; 53: 1289-1298.
122. Shu Z, He Y, Long T, Guo M, Xia Z, Fu X, *et al*. Is CXCR4-targeted 68Ga-pentixafor PET/CT a reliable AVS-free modality for surgical decision-making and prognostic prediction in primary aldosteronism with bilateral adrenal lesions? EJNMMI Res. 2025; 15: 111.
123. Zheng G, Liu S, Gao Y, Yan X, Wang W, Zhao Y, *et al*. 68Ga-pentixafor PET/CT versus adrenal venous sampling in guiding surgical management for primary aldosteronism: a prospective cohort study on postoperative outcomes. Int J Surg. 2026; 112: 844-853.
124. Rossi GP, Battistel M, Seccia TM, Rossi FB, Rossitto G. Subtyping of Primary Aldosteronism by Adrenal Venous Sampling. Endocr Rev. 2025; 46: 501-17.
125. Wu H, He H, Han T, Tian X, Zhu Z. Targeting cholesterol-dependent adrenal steroidogenesis for management of primary aldosteronism. Trends Endocrinol Metab. 2025; 36: 789-801.
126. Nayak SS, Amini-Salehi E, Joukar F, Biswas P, Nobakht S, Letafatkar N, *et al*. Cardiovascular and all-cause mortality outcomes of adrenalectomy versus medical treatment in primary aldosteronism: an umbrella review. Int J Surg. 2024; 110: 7367-80.
127. Tang R, Pu J, Huang Z. Clinical value of CXCR4-targeted PET-CT in primary aldosteronism: a systematic review and meta-analysis. Eur J Nucl Med Mol Imaging. 2025; 52: 4706-16.
128. Dillon BR, Agrawal N, Schwarz Y, Dancel-Manning K, Tabarin A, Lacroix A, *et al*. Update on Medical Treatment of Cushing's Syndrome. Drugs. 2025; 85: 1207-30.
129. Elenius H, Nieman LK. Diagnosis of Cushing's Disease. Endocrinol Metab Clin North Am. 2025; 54: 537-48.
130. Ding J, Tong A, Zhang Y, Zhang H, Huo L. Cortisol-Producing Adrenal Adenomas With Intense Activity on 68Ga-Pentixafor PET/CT. Clin Nucl Med. 2021; 46: 350-2.
131. Ghai A, Zheleznyak A, Egbulefu C, Blasi N, Black K, Tang R, *et al*. Chemo-RaST with bortezomib inhibits multiple myeloma relapse. Theranostics. 2025; 15: 9911-21.
132. Milrod CJ, Rubin L, Martinez B, Ollila TA, Olszewski AJ, Pelcovits A. Quality-of-life endpoints collection, reporting, and framing in randomised trials of indolent lymphomas: a systematic review. Lancet Haematol. 2025; 12: e312-7.
133. Cheson BD, Fisher RI, Barrington SF, Cavalli F, Schwartz LH, Zucca E, *et al*. Recommendations for initial evaluation, staging, and response assessment of Hodgkin and non-Hodgkin lymphoma: the Lugano classification. J Clin Oncol. 2014; 32: 3059-68.
134. Ngo HT, Leleu X, Lee J, Jia X, Melhem M, Runnels J, *et al*. SDF-1/CXCR4 and VLA-4 interaction regulates homing in Waldenstrom macroglobulinemia. Blood. 2008; 112: 150-8.
135. Hunter ZR, Yang G, Xu L, Liu X, Castillo JJ, Treon SP. Genomics, Signaling, and Treatment of Waldenström Macroglobulinemia. J Clin Oncol. 2017; 35: 994-1001.
136. Maddocks K. Update on mantle cell lymphoma. Blood. 2018; 132: 1647-56.
137. Annual clinical updates in hematological malignancies: a continuing medical education series. Am J Hematol. 2018; 93: E134.
138. Hosein PJ, Pastorini VH, Paes FM, Eber D, Chapman JR, Serafini AN, *et al*. Utility of positron emission tomography scans in mantle cell lymphoma. Am J Hematol. 2011; 86: 841-5.
139. Bodet-Milin C, Touzeau C, Leux C, Sahin M, Moreau A, Maisonneuve H, *et al*. Prognostic impact of 18F-fluoro-deoxyglucose positron emission tomography in untreated mantle cell lymphoma: a retrospective study from the GOELAMS group. Eur J Nucl Med Mol Imaging. 2010; 37: 1633-42.
140. Herndon TM, Chen SS, Saba NS, Valdez J, Emson C, Gatmaitan M, *et al*. Direct in vivo evidence for increased proliferation of CLL cells in lymph nodes compared to bone marrow and peripheral blood. Leukemia. 2017; 31: 1340-7.
141. Ostrom QT, Gittleman H, Truitt G, Boscia A, Kruchko C, Barnholtz-Sloan JS. CBTRUS Statistical Report: Primary Brain and Other Central Nervous System Tumors Diagnosed in the United States in 2011-2015. Neuro Oncol. 2018; 20: iv1-86.
142. Kreatsoulas D, Bolyard C, Wu BX, Cam H, Giglio P, Li Z. Translational landscape of glioblastoma immunotherapy for physicians: guiding clinical practice with basic scientific evidence. J Hematol Oncol. 2022; 15: 80.
143. Bian X wu, Yang S xin, Chen J hong, Ping Y fang, Zhou X dong, Wang Q liang, *et al*. Preferential expression of chemokine receptor CXCR4 by highly malignant human gliomas and its association with poor patient survival. Neurosurgery. 2007; 61: 570-8.
144. Lv B, Yang X, Lv S, Wang L, Fan K, Shi R, *et al*. Retraction Note to: CXCR4 Signaling Induced Epithelial-Mesenchymal Transition by PI3K/AKT and ERK Pathways in Glioblastoma. Mol Neurobiol. 2017; 54: 2380.
145. Kligerman MP, Sethi RKV, Kozin ED, Gray ST, Shrime MG. Morbidity and mortality among patients with head and neck cancer in the emergency department: A national perspective. Head Neck. 2019; 41: 1007-15.
146. Bray F, Laversanne M, Sung H, Ferlay J, Siegel RL, Soerjomataram I, *et al*. Global cancer statistics 2022: GLOBOCAN estimates of incidence and mortality worldwide for 36 cancers in 185 countries. CA Cancer J Clin. 2024; 74: 229-63.
147. Victora GD, Nussenzweig MC. Germinal Centers. Annu Rev Immunol. 2022; 40: 413-42.
148. Sivarajah S, Isaac A, Cooper T, Zhang H, Puttagunta L, Abele J, *et al*. Association of Fludeoxyglucose F 18-Labeled Positron Emission Tomography and Computed Tomography With the Detection of Oropharyngeal Cancer Recurrence. JAMA Otolaryngol Head Neck Surg. 2018; 144: 1037-43.

149. Vaidya P, Khorrami M, Bera K, Fu P, Delasos L, Gupta A, *et al.* Computationally integrating radiology and pathology image features for predicting treatment benefit and outcome in lung cancer. NPJ Precis Oncol. 2025; 9: 161.
150. Doroudian M, Abbasgholinejad E, Soezi M. Advancements in gene therapy for lung cancer: from genetic insights to clinical applications. QJM. 2025; 118: 631-5.
151. Watts A, Singh B, Basher R, Singh H, Bal A, Kapoor R, *et al.* 68Ga-Pentixafor PET/CT demonstrating higher CXCR4 density in small cell lung carcinoma than in non-small cell variant. Eur J Nucl Med Mol Imaging. 2017; 44: 909-10.
152. Shim H, Lau SK, Devi S, Yoon Y, Cho HT, Liang Z. Lower expression of CXCR4 in lymph node metastases than in primary breast cancers: potential regulation by ligand-dependent degradation and HIF-1alpha. Biochem Biophys Res Commun. 2006; 346: 252-8.
153. Kaemmerer D, Träger T, Hoffmeister M, Sipos B, Hommann M, Sänger J, *et al.* Inverse expression of somatostatin and CXCR4 chemokine receptors in gastroenteropancreatic neuroendocrine neoplasms of different malignancy. Oncotarget. 2015; 6: 27566-79.
154. Döring Y, Pawig L, Weber C, Noels H. The CXCL12/CXCR4 chemokine ligand/receptor axis in cardiovascular disease. Front Physiol. 2014; 5: 212.
155. Lapa C, Reiter T, Werner RA, Ertl G, Wester HJ, Buck AK, *et al.* [(68)Ga]Pentixafor-PET/CT for Imaging of Chemokine Receptor 4 Expression After Myocardial Infarction. JACC Cardiovasc Imaging. 2015; 8: 1466-8.
156. Thackeray JT, Derlin T, Haghikia A, Napp LC, Wang Y, Ross TL, *et al.* Molecular Imaging of the Chemokine Receptor CXCR4 After Acute Myocardial Infarction. JACC Cardiovasc Imaging. 2015; 8: 1417-26.
157. Tran HH, Yamaguchi A, Manning HC. Radiotheranostic landscape: A review of clinical and preclinical development. Eur J Nucl Med Mol Imaging. 2025; 52: 2685-709.
158. Zhang S, Wang X, Gao X, Chen X, Li L, Li G, *et al.* Radiopharmaceuticals and their applications in medicine. Signal Transduct Target Ther. 2025; 10: 1.
159. Moreno-Alcántar G, Drexler M, Casini A. Assembling a new generation of radiopharmaceuticals with supramolecular theranostics. Nat Rev Chem. 2024; 8: 893-914.
160. Wei Z, Li B, Wen X, Jakobsson V, Liu P, Chen X, *et al.* Engineered Antibodies as Cancer Radiotheranostics. Adv Sci (Weinh). 2024; 11: e2402361.
161. Song Y, Zou J, Castellanos EA, Matsuura N, Ronald JA, Shuhendler A, *et al.* Theranostics - a sure cure for cancer after 100 years? Theranostics. 2024; 14: 2464-88.
162. Morgan KA, Rudd SE, Noor A, Donnelly PS. Theranostic Nuclear Medicine with Gallium-68, Lutetium-177, Copper-64/67, Actinium-225, and Lead-212/203 Radionuclides. Chem Rev. 2023; 123: 12004-35.
163. Xu J, Chen J, Song S, Song L, Wang R, Hao J, *et al.* 177Lu-Dotatate versus high-dose long-acting octreotide for the treatment of patients with advanced, grade 1-2, well-differentiated gastroenteropancreatic neuroendocrine tumours (XT-XTR008-3-01): an open-label, randomised, phase 3 trial. Ann Oncol. 2025; 04697-6.
164. Herr FL, Dascalescu C, Ebner R, Schnitzer ML, Fabritius MP, Schmid-Tannwald C, *et al.* Association of integrated biomarkers and progression-free survival prediction in patients with gastroenteropancreatic neuroendocrine tumors undergoing [177Lu]Lu-DOTA-TATE therapy. Theranostics. 2025; 15: 6444-53.
165. Karpinski MJ, Hoberück S, Fendler WP, Civan C, Bundschuh RA, Thomas C, *et al.* Association Between the PRIMARY Score at Staging Prostate-specific Membrane Antigen Positron Emission Tomography and Overall Survival Among Patients with Newly Diagnosed Prostate Cancer: Findings from the International, Multicenter PROMISE Registry. Eur Urol. 2025; 04773-6.
166. Fettke H, Kostos L, Docanto M, Bukczynska P, Ng N, Medhurst E, *et al.* Baseline and Early On-treatment Circulating Tumour DNA Fraction Are a Key Prognostic Biomarker in Metastatic Castration-resistant Prostate Cancer Treated with [177Lu]Lu-PSMA-617. Eur Urol. 2025; 00501-9.
167. Lapa C, Lückerath K, Kircher S, Hänscheid H, Grigoleit GU, Rosenwald A, *et al.* Potential influence of concomitant chemotherapy on CXCR4 expression in receptor directed endoradiotherapy. Br J Haematol. 2019; 184: 440-3.
168. Maurer S, Herhaus P, Lippenmeyer R, Hänscheid H, Kircher M, Schirbel A, *et al.* Side Effects of CXC-Chemokine Receptor 4-Directed Endoradiotherapy with Pentixather Before Hematopoietic Stem Cell Transplantation. J Nucl Med. 2019; 60: 1399-405.
169. Lapa C, Hänscheid H, Kircher M, Schirbel A, Wunderlich G, Werner RA, *et al.* Feasibility of CXCR4-Directed Radioligand Therapy in Advanced Diffuse Large B-Cell Lymphoma. J Nucl Med. 2019; 60: 60-4.
170. Hänscheid H, Schirbel A, Hartrampf P, Kraus S, Werner RA, Einsele H, *et al.* Biokinetics and Dosimetry of 177Lu-Pentixather. J Nucl Med. 2022; 63: 754-60.
171. Dreher N, Dörrler AL, Kraus S, Higuchi T, Serfling SE, Samnick S, *et al.* C-X-C Motif Chemokine Receptor 4-Targeted Radioligand Therapy in Hematological Malignancies-Myeloablative Effects, Antilymphoma Activity, and Safety Profile. Clin Nucl Med. 2024; 49: 146-51.
172. Braitsch K, Lorenzini T, Hefter M, Koch K, Nickel K, Peeken JC, *et al.* CXCR4-directed endoradiotherapy with [177Lu]Pentixather added to total body irradiation for myeloablative conditioning in patients with relapsed/refractory acute myeloid leukemia. Theranostics. 2025; 15: 19-29.
173. Fath MA, Liu D, Ewald JT, Robles-Planells C, Tomanek-Chalkley AM, Graves SA, *et al.* Chemokine Receptor CXCR4 Radioligand Targeted Therapy Using 177Lutetium-pentixather for Pulmonary Neuroendocrine Cancers. Radiat Res. 2024; 201: 35-47.
174. Taghizadehasl M, Prasad V, Roustaei H, Ghodsirad M. Chemokine receptor-4-targeted imaging with [68Ga]Ga-Pentixafor PET: unveiling its diagnostic and prognostic potential across cancers: a systematic review. Nucl Med Commun. 2025; 46: 1131-44.
175. Liao M, Wu J, Dai T, Liu G, Zhang J, Zhu Y, *et al.* CXCR4: A Promising Novel Strategy for Lung Cancer Treatment. Biomolecules. 2026; 16: 188.
176. Yang B, Shan C, Lin Z, Hu M, Qin C, Zeng D, *et al.* Preparation and evaluation of a novel albumin-binding heterodimer therapeutic radiopharmaceutical with remarkable tumor accumulation and retention. Eur J Med Chem. 2025; 290: 117589.
177. Zhang X, Yang B, Qin C, Song X, Lv X, Zeng D, *et al.* Clinical Translation of a Dual-Integrin αvβ3- and CD13-Targeting PET Tracer. Clin Nucl Med. 2025; 50: 332-7.
178. Yang B, Shan C, Lv X, Song X, Zeng D, An R, *et al.* 177Lu-Labeled Heterodimeric Agent with High Stability Targeting Neovascularization for Tumor Radioligand Therapy. J Med Chem. 2025; 68: 3146-56.
179. Zhang X, Fang H, Yang B, Qin C, Hu F, Ruan W, *et al.* Phase I study of [68Ga]Ga-HX01 for targeting integrin αvβ3 and CD13 in healthy and malignancy subjects. Eur J Nucl Med Mol Imaging. 2025; 52: 1293-304.
180. Yang B, Shan C, Song X, Lv X, Long Y, Zeng D, *et al.* Development and evaluation of albumin binder-conjugated heterodimeric radiopharmaceuticals targeting integrin αvβ3 and CD13 for cancer therapy. Eur J Nucl Med Mol Imaging. 2024; 51: 3334-45.
181. Yu X, Li H, Ou H, Ma L, Yu K, Li G, *et al.* 68Ga/161Tb-Labeled CXCR4-Targeted Probe with Enhanced Positive Charge: Improved Affinity and Longer Tumor Retention without Survival Benefit in Mice Models. J Med Chem. 2026.
182. Rahimian S, Najafi H, Doroudian M. CXCR4-targeted theranostics in acute leukemia: disrupting leukemic cell-microenvironment interactions with pentixafor and pentixather. Med Oncol. 2025; 42: 402.
183. Osl T, Schmidt A, Schwaiger M, Schottelius M, Wester HJ. A new class of PentixaFor- and PentixaTher-based theranostic agents with enhanced CXCR4-targeting efficiency. Theranostics. 2020; 10: 8264-80.
184. Rajendran A, Elumalai V, Balasubramaniyam S, Elumalai K. C-X-C chemokine receptor type 4 (CXCR4) antagonism in precision oncology: Clinical applications and future directions. Cancer Pathog Ther. 2026; 4: 208-18.
185. Keenan BP, Yadav M, Ansstas G, Fabrizio D, Murugesan K, Montesion M, *et al.* Intratumoral heterogeneity and immunotherapy resistance: clinical implications. Ann Oncol. 2025; 06217-9.
186. Zhou K, Liu X, Zhu H. Overcoming resistance to antibody-drug conjugates: from mechanistic insights to cutting-edge strategies. J Hematol Oncol. 2025; 18: 96.
187. Zhang W, Li Y, Zhou MM, Zeng L. Targeting BRD4 bromodomains and beyond: exploring new therapeutic frontiers. Trends Pharmacol Sci. 2025; 00224-X.
188. Chen X. From Quantum Dots to Cancer Nanotheranostics. Nano Lett. 2025; 25: 13967-9.